Technical insights into fluorescence lifetime microscopy of mechanosensitive Flipper probes.

Chloé Roffay[1], Juan Manuel García-Arcos[1], Pierrik Chapuis[1], Javier López-Andarias[2,3], Falk Schneider[4], Adai Colom[5,6,7], Caterina Tomba[8], Ilaria Di Meglio[1], Valentin Dunsig9, Stefan Matile[2,3], Aurélien Roux[1,3]*, Vincent Mercier[1,3]*

[1]Department of Biochemistry, University of Geneva, CH-1211 Geneva, Switzerland.
[2]Department of Organic Chemistry, University of Geneva, CH-1211 Geneva, Switzerland
[3]National Center of Competence in Research in Chemical Biology, University of Geneva, CH-1211 Geneva, Switzerland.
[4] Translational Imaging Center, University of Southern California, Los Angeles, California 90089, United States of America
[5] Biofisika Institute (CSIC, UPV/EHU), 48940 Leioa, Spain;
[6] Department of Biochemistry and Molecular Biology, Faculty of Science and Technology, Campus Universitario, University of the Basque Country (UPV/EHU), 48940 Leioa, Spain
[7] IKERBASQUE, Basque Foundation for Science, 48013 Bilbao, Spain
[8] Univ Lyon, CNRS, INSA Lyon, Ecole Centrale de Lyon, Université Claude Bernard Lyon 1, CPE Lyon, INL, UMR 5270, Villeurbanne 69622, France
[9] Aix-Marseille Université & CNRS, IBDM - UMR7288 & Turing Centre for Living Systems, Marseille, France

*correspondence to: aurelien.roux@unige.ch, vincent.mercier@unige.ch;

Abstract: Measuring forces within living cells remains a technical challenge. We developed hydrophobic mechanosensing fluorescent probes called Flippers, whose fluorescence lifetime depends on lipid packing and can report on membrane tension. Here, we describe technical optimization of the probe imaging, and diverse characterizations in various biological and in vitro systems. We provide a guideline to measure biophysical parameters of cellular membranes by FLIM microscopy with Flipper probes, providing evidences that flippers can report long range forces in cells, tissues and organs[i].

Introduction

Measuring physical forces in biological material is of increasing interest, but remains technically challenging[1]. The possibility of measuring such forces through microscopy imaging presents the advantages of being less intrusive than many mechanical methods, making use of the universally available microscopy equipment in research labs. Many fluorescence tools have been developed in this regard, in particular Forster Resonance Energy Transfer (FRET) biosensors, in which the elongation of a linker between two FRET fluorophores under force

reduces FRET efficiency. The FRET couple and the linker can be composed of fluorescent proteins connected by a peptide chain, all being easily expressed in cells using standard molecular biology techniques. This has been developed to measure forces at focal adhesions, and has been extended to measure force between membranes and actin[2], the cytoskeleton and the nucleoskeleton[3] or under shear stress[4]. However, these biosensors have several limitations, namely that the force range is very small, and thus require the use of several chimeric constructs with different linkers. Also, it requires the force sensor to be bound to proteins "handles" onto which the force is applied and finding the right combination of interacting domains that will not detach under force remains challenging.

Another strategy has been to design small chemicals whose fluorescence properties will change under force variation. For example, molecular rotors based on Fluorescence Lifetime Imaging Microscopy (FLIM) were designed to measure viscosity in membranes[5,6]. One of the challenges has been to expand the list of forces that can be measured, as some of the forces are exerted within materials, and not between materials. We have designed, synthesized and characterized small-molecules called FLIPPERS that can report changes of membrane lateral forces due to lipid packing variations through changes of their conformation and hence of their fluorescence properties[7]. The high sensitivity of Flippers allows them to report membrane tension variations by changes of the lifetime of their excited state or fluorescence lifetime[8], upon osmotic shocks[9,10] or to investigate cellular processes such as lysosomal exocytosis[11]. Over the past six years, we designed various derivatives targeting different organelles[12] (plasma membrane, endoplasmic reticulum, mitochondria and lysosome/late endosome). We also developed probes with different biochemical and/or photochemical properties[6] (HaloFlipper, HaloPhotoFlipper, HydroFlipper). We identified fluorescence lifetime imaging (FLIM) as the best way to report the conformational changes of Flipper probes with lipid packing. However, measuring membrane tension using FLIM of Flippers remains technically challenging. This method paper provides technical and practical information to make the use of Flipper probes for membrane tension measurements more accessible and reproducible.

I-Basics of Flipper probes

Four commercialized Flipper probes with identical mechano-chemistry principle target different membranes in cells: Flipper-TR for plasma membrane, ER Flipper-TR for endoplasmic reticulum, Lyso Flipper-TR for late endo/lysosomes and Mito Flipper-TR for mitochondria. The common chemical structure of Flipper probes (see Fig 1a) is composed of

FIGURE 1

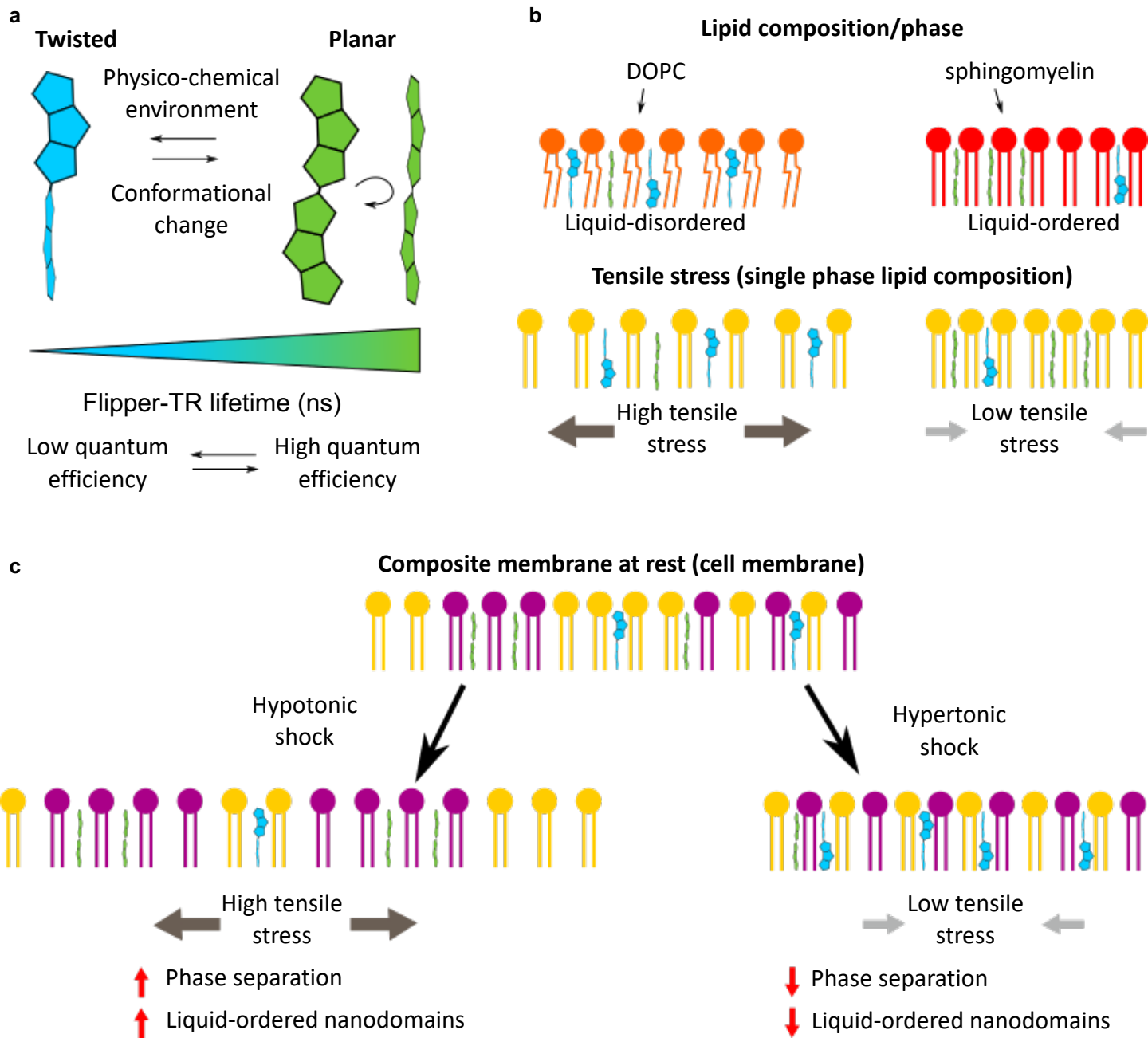
a
Twisted
Planar
Physico-chemical environment
Conformational change
Flipper-TR lifetime (ns)
Low quantum efficiency
High quantum efficiency
b
Lipid composition/phase
DOPC
sphingomyelin
Liquid-disordered
Liquid-ordered
Tensile stress (single phase lipid composition)
High tensile stress
Low tensile stress
c
Composite membrane at rest (cell membrane)
Hypotonic shock
Hypertonic shock
High tensile stress
Low tensile stress
Phase separation
Liquid-ordered nanodomains
Phase separation
Liquid-ordered nanodomains

Figure 1: Principle of Flipper probe

(a) Flipper design is a planarizable push-pull system. Mechanical planarization is responsible for a spectrum of configurations from planar to twisted configuration, which will affect the photo-physics and notably the time of the excited state of the probe

(b) Lateral forces within the membrane directly set the twisting and therefore the photo-physics of the Flipper probes.

(c) In complex membrane (e.g cell membranes), high tensile stress will trigger phase separation and the formation of highly packed membrane nanodomains reported by an increase of Flippers lifetime.

41 two dithienothiophenes (DTT) fluorescent groups that can rotate around the carbon bond that
42 links them together. Methyl groups have been added at specific places to ensure that the two
43 DTT groups are twisted out of co-planarity in the ground state but can still be planarized under
44 application of orthogonal forces. Thus, Flippers have been designed as molecular sensors for
45 compressive forces.
46 As the Flipper structure is mostly hydrophobic, the molecule spontaneously inserts in between
47 hydrophobic tails of lipids that constitute cellular membranes (Fig 1b). When inserted, the
48 hydrophobic forces that pack the lipids into a bilayer exert pressure onto the Flipper
49 fluorophore and planarize it. Its planarization depends on the lipid composition, and in short,
50 more ordered membranes exert more force and provide more planarization of Flippers and
51 reversely, disordered membrane, less force and planarization.
52 The conformation (i.e. how much the Flipper molecule is planarized versus twisted) of the
53 Flipper affects several parameters of the photo-physics of the molecule: in the planarized state,
54 the photon emission efficiency is increased by 10x compared to the most twisted state, and the
55 peak of photon absorption is shifted towards larger wavelength, while the change is minimal
56 for the emission peak [13].
57 In particular, we noted that the lifetime of Flipper dramatically varied with lipid composition.
58 The lifetime (τ_1 or the longest decay of a bi-exponential fit) in the twisted state, equivalent to
59 highly disordered lipid membranes, was as small as 2.3 ns, while it could reach values as high
60 as 7 ns in highly ordered membranes, where the molecule is fully planarized. This large range
61 of lifetime values is due to the fact that in the planarized state, fluorescence of the two
62 fluorophores is coupled through an electron transfer from the donor group to the acceptor
63 group[6], which delays emission of the photons, giving longer lifetimes.
64 The range of lifetime values that this probe could cover was impressively large compared to
65 other probes. For comparison, the lifetime of the Green Fluorescent Protein hardly varies
66 around 2 ns[14]. We thus imagined that the Flippers are so sensitive that they could report tiny
67 changes of the hydrophobic pressure linked to changes of membrane tension. In cell
68 membranes or in GUVs with phase separating lipid composition, increasing tension results in
69 lifetime increase and decreasing tension results in a shorter lifetime. This is likely due to a
70 tension induced lipid phase separation and membrane reorganization in highly ordered
71 microdomains (Fig 1c). These observations have been confirmed in many studies[1,44,48-50] and
72 validated by molecular simulation[15]. Flipper is thus complementary to Laurdan, an organic
73 fluorescent maker which allows by measuring its fluorescence anisotropy to detect changes in

plasma membrane fluidity. Since Flippers lifetime changes with both the lipid composition and membrane tension, changes of the lifetime can be directly associated with a change in membrane tension only in cases where lipid composition is not changing. While this condition is always met *in vitro*, in cells, we usually consider that any variation of lifetime on the second timescale is related to membrane tension, as lipid composition hardly changes over this timescale. For longer timescales (minute, hour), appropriate controls that the lipid composition is not dramatically changing are required.

II-Staining biological samples with Flipper probes

Being hydrophobic, the probe is in the micellar form in aqueous solutions and is not fluorescent in this state. When the Flipper probe diffuses within lipid membranes, it inserts vertically between lipids and fluoresces. Thus, Flipper probes are "fluorogenic", becoming fluorescent only when inserted in the structure they target. We describe staining procedures, problems and solutions below.

A-Staining of cultured cells

To label most of the cell lines tested (Fig 2a), the probe, solubilized in DiMethylSulfOxide (DMSO), was normally directly added to the imaging medium at 1 µM final concentration and incubated 15 min at 37°C with cells. MDCK-II cell medium was replaced 1 h before imaging with medium containing 1 mM of Flipper-TR in order to allow the probe to penetrate through the cell monolayer (and, when relevant, the alginate wall). To keep a low concentration of DMSO in the final medium, 1 mM stock solutions of Flipper probes were usually made. In some cell types (MDCK, HeLa Kyoto and MZ), 5 min of Flipper incubation at 37°C might be enough to obtain good staining. However, at high cell density or in 3D cell cultures and tissues, longer incubation - in the order of a few hours - may be necessary. Imaging medium (Fluorobrite with HEPES or CO_2 supply, or Leibovitz if no CO_2 supply is available) was usually used and gave a good signal over noise ratio. The use of Foetal Bovine Serum (FBS) during staining and imaging can cause a lower signal, as it contains proteins which can extract hydrophobic molecules from membranes such as Albumin. However, we haven’t observed a dramatic change of labelling efficiency using solutions described above supplemented with FBS. If the staining appears to be low with FBS, we nevertheless recommend testing solutions without it. We did not observe drastic differences on the fluorescence intensity and lifetime of

FIGURE 2

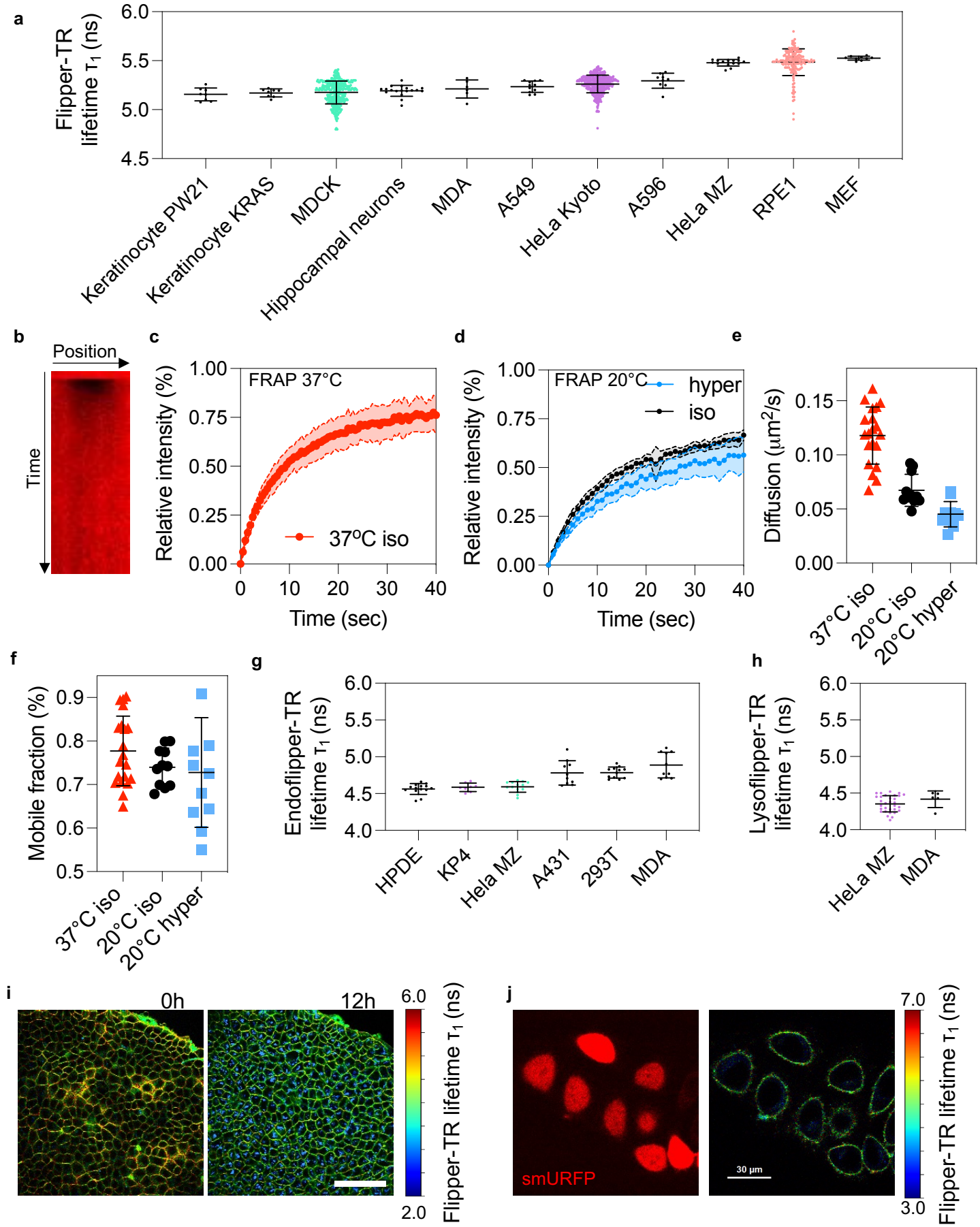
a
Flipper-TR lifetime τ1 (ns)
6.0
5.5
5.0
4.5
Keratinocyte PW21
Keratinocyte KRAS
MDCK
Hippocampal neurons
MDA
A549
HeLa Kyoto
A596
HeLa MZ
RPE1
MEF
b
Position
Time
c
FRAP 37°C
Relative intensity (%)
1.00
0.75
0.50
0.25
0.00
37°C iso
0
10
20
30
40
Time (sec)
d
FRAP 20°C
hyper
iso
Relative intensity (%)
Time (sec)
e
Diffusion (μm²/s)
0.15
0.10
0.05
0.00
37°C iso
20°C iso
20°C hyper
f
Mobile fraction (%)
0.9
0.8
0.7
0.6
0.5
37°C iso
20°C iso
20°C hyper
g
Endoflipper-TR lifetime τ1 (ns)
6.0
5.5
5.0
4.5
4.0
HPDE
KP4
Hela MZ
A431
293T
MDA
h
Lysoflipper-TR lifetime τ1 (ns)
HeLa MZ
MDA
i
0h
12h
6.0
2.0
Flipper-TR lifetime τ1 (ns)
j
smURFP
30 μm
7.0
3.0
Flipper-TR lifetime τ1 (ns)

Figure 2: General behavior of Flipper probes

(a) Graph showing the Flipper-TR lifetime ($\tau 1$) extracted from different cell types

(b) Kymograph showing the recovery of Flipper-TR signal after bleaching at the plasma membrane (FRAP experiment)

(c) Graph showing FRAP curves of Flipper-TR at the plasma membrane at 37°C on HeLa cells in isotonic medium (n = 18)

(d) Graph showing FRAP curves of Flipper-TR at the plasma membrane at 22°C on HeLa cells in isotonic (320 mOsm) medium (n = 11) versus hypertonic (800 mOsm) medium (n = 10)

(e) Graph showing diffusion time coefficients (μm^2/sec) extracted from graph (d) data

(f) Graph showing the mobile fractions (%) extracted from graph (d) data

(g) Graph showing the Lyso Flipper lifetime (τ_1) extracted from different cell types (n>5 fields of view with at least 5 cells per field for each condition)

(h) Graph showing the Endo Flipper lifetime (τ_1) extracted from different cell types (n>5 field of view with at least 5 cells per field for each condition)

(i) FLIM images showing MDCK tissue stained with Flipper-TR at different timepoints.

(j) Flipper-TR FLIM and confocal image of HeLa cells labelled with Flipper-TR lifetime and smURFP fluorescence

107 the probe between cells imaged at 37°C and the ones imaged at room temperature. Similarly,
108 CO_2 adjunction in the imaging chamber or working with a medium supplemented with HEPES
109 does not significantly impact Flipper fluorescence intensity or lifetime.
110
111 Importantly, the cell labelling occurs through a dynamic equilibrium of the probe with the
112 micellar pool in the cell culture medium. Thus, a constant exchange of Flipper-TR between the
113 plasma membrane and the medium occurs. This exchange is rapid for the Flipper-TR because
114 the medium is directly in contact with the plasma membrane labelled by the probe. Using
115 FRAP, we detected a faster diffusion coefficient D at 37°C, D= 0.12 +/- 0.04 μm^2/sec (mobile
116 fraction of 78% +/- 5) (Fig 2b, c) than at 20°C, D=0.07 +/- 0.02 μm^2/sec (Fig 2d, e). As
117 expected, a decrease of plasma membrane tension induced by hypertonic treatment reduces the
118 Flipper-TR diffusion coefficient at room temperature from 0.07 +/- 0.02 μm^2/sec to 0.05 +/-
119 0.01 μm^2/sec (Fig 2e) without significantly impacting the mobile fraction (Fig 2f).
120 We recommend, if possible, to keep a constant Flipper-TR concentration along the experiment.
121 Concerning Lyso Flipper-TR, the molecule diffuses freely across the plasma membrane and
122 quickly concentrates in the membrane of late endosomes and lysosomes (in a few minutes)
123 after headgroup protonation in this acidic environment. Consequently, for short timescale
124 experiments (less than 2h) it is not an issue to leave cells in Flipper medium containing Lyso
125 Flipper-TR. However, loss of the acidity of endosomal compartments after treatments or
126 change in the pH of the medium (due for example to phototoxicity) may trigger loss of the
127 Lyso Flipper-TR staining. The best labelling was obtained by incubating Lyso Flipper-TR at 1
128 µM in Fluorobrite medium without serum for 20 minutes at 37°C prior to imaging.
129
130 Because of the dynamic exchange of the probe between the membrane and the medium,
131 washing Flipper labelled cells with medium containing FBS or BSA will decrease Flipper-TR
132 staining. Therefore, if washing is absolutely needed, it is recommended to wash with medium
133 without FBS, and/or keeping the concentration of the Flipper constant in the washes, which
134 will limit the decrease of the membrane signal.
135 Reaching the dynamic equilibrium takes about 5-10 minutes, thus the photon count depends
136 on the time of incubation of cells with the probe, until it reaches a plateau value that depends
137 on your system. Incubations that are too long may lead to Flipper-TR endocytosis and
138 endosomal labelling. The Flipper-TR lifetimes within endosomal compartments are notably
139 lower than in the plasma membrane (Fig 2g, h), and we have never observed Flipper-TR

labelling expanding further away than from the endosomes (probably even the early endosomes). Also, the Flipper-TR endosomal labelling appeared with various times depending on the cell types and experimental conditions. In MDCK, we observed that endocytosis occurred after 12 hours (Fig 2i).

For long-term imaging experiments (several hours) with sufficient time-lapse between images, we recommend performing sample-labelling for each time point: the sample is incubated with Flipper-TR, imaged, and then the probe is washed away using medium with BSA or FBS. Each timepoint requires re-incubation of the probe to prevent Flipper-TR endocytosis.

B-Co-staining with Flipper-TR

In order to specifically analyse the tension or lipid composition of a given organelle or during a biological process, it is possible to use other fluorescent probes or stable cell lines in conjunction with Flipper-TR. However, to avoid any fluorescence overlap with the probe, which could affect lifetime measurements, blue or far-red fluorescent probes should be used (e.g: Organic dyes like Alexa-405 or Alexa-647 or Blue fluorescent protein, E2-Crimson or smURFP for fusion proteins, see Fig 2j). Indeed, due to the configuration of the probe (two heads), Flipper-TR has a large spectrum of emission and a large spectrum of absorption. The excitation peak of Flipper is at 485 nm and fluorescence emission is collected using a band pass 600/50 emission filter. Therefore, for example in the case of an organelle labelled with Alexa-405, excitation of this fluorophore (peak at 400 nm) will only weakly excite Flipper-TR, limiting the phototoxicity while the emission of Alexa-405 (400-530 nm) will not go through the FLIM detector and will not interfere with Flipper-TR lifetime measurement.

C-List of cells and organisms from which we obtained successful staining and imaging using Flipper probes

<u>List of cell types used with Flipper-TR</u>: HeLa MZ, HeLa Kyoto, MDCK, keratinocyte PW21, keratinocyte KRAS, hippocampal neurons, MDA, A549, A596, RPE1, MEF with lifetime value (tau1) ranging from 5 ns to 5.7 ns (Fig 2a).

<u>List of cell types used with Lyso-Flipper-TR</u>: HPDE, KP4, Hela MZ, A431, 293T, MDA with lifetime value (τ_1) ranging from 4.4 ns to 5.1 ns (Fig 2g).

FIGURE 3

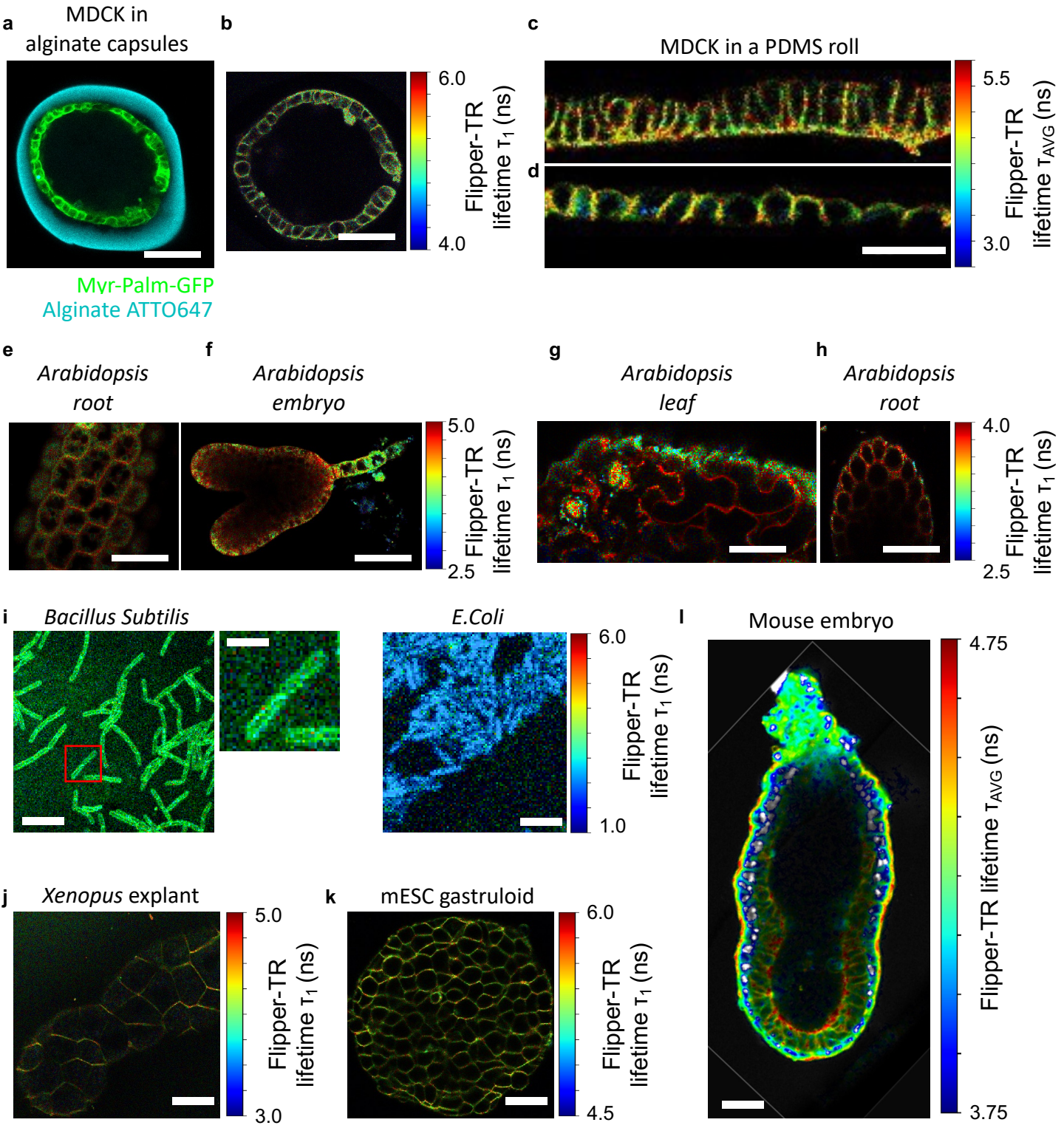
a
MDCK in alginate capsules
Myr-Palm-GFP
Alginate ATTO647
b
6.0
4.0
Flipper-TR lifetime τ1 (ns)
c
MDCK in a PDMS roll
d
5.5
3.0
Flipper-TR lifetime τAVG (ns)
e
Arabidopsis root
f
Arabidopsis embryo
5.0
2.5
Flipper-TR lifetime τ1 (ns)
g
Arabidopsis leaf
h
Arabidopsis root
4.0
2.5
Flipper-TR lifetime τ1 (ns)
i
Bacillus Subtilis
E.Coli
6.0
1.0
Flipper-TR lifetime τ1 (ns)
l
Mouse embryo
4.75
3.75
Flipper-TR lifetime τAVG (ns)
j
Xenopus explant
5.0
3.0
Flipper-TR lifetime τ1 (ns)
k
mESC gastruloid
6.0
4.5
Flipper-TR lifetime τ1 (ns)

Figure 3: Flipper probes staining in various model and organisms

(a) Representative fluorescence image of a MDCK monolayer in an alginate capsule (Myr-Palm-GFP stain the MDCK cells and ATTO647 stain the alginate capsule in blue). Scale bar is 50 μm.

(b) Representative FLIM image of an MDCK monolayer stained with Flipper-TR in an alginate capsule. Scale bar is 50 μm.

(c) Representative FLIM bottom view of an MDCK monolayer stained with Flipper-TR in a PDMS roll.

(d) Representative FLIM side view of an MDCK monolayer stained with Flipper-TR in a PDMS roll. Scale bar is 20 μm.

(e) Representative FLIM image of Arabidopsis root stained with Flipper-TR. Scale bar is 20 μm.

(f) Representative FLIM image of the entire Arabidopsis embryo stained with Flipper-TR. Scale bar is 40 μm.

(g) Representative FLIM image of Arabidopsis leaf stained with Flipper-TR. Scale bar is 20 μm.

(h) Representative FLIM image of Arabidopsis root stained with Flipper-TR. Scale bar is 40 μm.

(i) Representative FLIM image of Gram-positive (B. subtilis) stained with Flipper-TR and representative FLIM image of Gram-negative (E. coli) stained with Flipper-TR showing a non-specific signal. Scale bar is 10 μm.

(j) Representative FLIM image of Xenopus explant stained with Flipper-TR. Scale bar is 100 μm.

(k) Representative FLIM image of mESC gastruloid stained with Flipper-TR. Scale bar is 80 μm.

(l) Representative FLIM image in E6.5 mouse embryos stained with Flipper-TR. Scale bar is 20 μm.

173 List of cell types used with Endo Flipper-TR: HeLa MZ, MDA with lifetime value (τ_1) ranging
174 from 4.1 ns to 4.7 ns (Fig 2h).
175 List of organisms stained with Flipper-TR: alginate capsules containing cells, PDMS tubes
176 with attached cells on the inner surface, Arabidopsis thaliana leaf, Arabidopsis thaliana plant
177 root, Bacillus Subtilis (Fig 3i), Xenopus explant (Fig 3j), 3D gastruloids of mESC (Fig 3k) or
178 mouse embryos (Fig 3l and ref[16]).
179
180 List of organisms where Flipper-TR staining does not work: E.Coli (gramm – cells) (Fig 3i,
181 right panel). E.Coli showed only background Flipper-TR staining when compared to Bacillus
182 Subtilis, suggesting that the presence of a cell wall in gram negative bacteria could prevent
183 Flipper-TR staining. Different attempts were made by several groups to stain zebrafish but they
184 were unsuccessful so far.
185

186 D-Different probes for different staining

187
188 Various derivatives of Flipper were developed to target the endoplasmic reticulum (ER Flipper-
189 TR), the mitochondria (Mito Flipper-TR), the lysosome/late endosome (Lyso Flipper-TR)[12]
190 and more recently the early endosome (Endo Flipper-TR)[17] as well as a version of the probe
191 for single-molecule super-resolution imaging of membrane tension (SR-Flipper[18,19]). The
192 structures can be found in[6]. The ER Flipper-TR selectively labels the membranes of
193 endoplasmic reticulum via a pentafluorophenyl group which reacts with cysteine of proteins
194 present on ER outer surface. The average lifetime of ER Flipper-TR is lower (3.5 ns in HeLa
195 cells) than Flipper-TR (4.5 ns in HeLa cells) in various cell lines. The Mito Flipper-TR
196 selectively labels the membranes of mitochondria via the interaction between the hydrophobic
197 triphenylphosphonium cation with the negatively charged surface and the inside negative
198 potential of the mitochondrial membrane. As observed for ER Flipper-TR, the average lifetime
199 of Mito Flipper-TR is rather low (around 3.2 ns in HeLa cells).
200 Lyso Flipper-TR and Endo Flipper TR contain a morpholine headgroup of higher pKa in Endo
201 Flipper-TR compared to Lyso Flipper-TR. This morpholine group is protonated in the acidic
202 environment of endosomes and retained in its membrane. The average lifetime of Lyso Flipper-
203 TR is around 4 ns in HeLa cells. Endo and Lyso Flipper-TR are showing very weak
204 phototoxicity.
205 SR-Flipper is behaving as Flipper-TR (labelling plasma membrane in cells) and is reversibly
206 switching from bright-state ketones to dark-state hydrates, hemiacetals, and hemithioacetals

both in twisted and planarized state. It is therefore possible to use it for single-molecule localization microscopy and to resolve membranes well below the diffraction limit. The lifetime (τ_1) of SR-Flipper is usually slightly lower (~10%) than the lifetime of Flipper-TR. HaloFlipper is based on the combination of the Flipper and a Halo tag to label any membrane of interest by targeting membrane specific protein labelled with a halo tag. Halo PhotoFlipper targets the nuclear membrane and the inner plasma membrane using a photocleavable domain[20].

III-Acquisition

Flipper probes have long average fluorescence lifetimes, up to 7 ns depending on membrane composition, which means that photons with lifetime up to 50 ns can be detected. Consequently, FLIM systems with sampling frequencies of 20 MHz are the best devices to use in order to detect all the photons allowing for most accurate TCSPC fits. We found however that the dye can also be efficiently excited using a two-photon mechanism (excitation around 880 nm – 950 nm, Fig S1a, b). Unfortunately, most two-photon microscope set-ups are only equipped with a fixed repetition rate laser pulsing at 80 MHz. Increasing the pulse rate leads to artificially shortened lifetimes in GUVs (excited with one-photon at 488 nm) (FigS1c, d, e). While the lifetime of Flipper-TR in GUVs still depends on the membrane compositions, the dynamic range is reduced at 80 MHz compare to 20 MHz (FigS1,c,d,e). The use of Flipper-TR in conjunction with the possibility of two-photon excitation is a promising feature for *in vivo* studies and deep tissue imaging of tension.

On PicoQuant systems the pulsed laser frequency can be set between 80 MHz and 31.25 kHz, but LEICA systems are by default 80 MHz which will not allow to measure lifetimes higher than 12.5 ns. Therefore, the sampling frequency has to be reduced in LEICA systems, using the pulse-picker device (illuminates one out of 2 or more laser pulses), otherwise the lifetime will be underestimated.

Because of the bi-exponential nature of the Flipper decay curve, it is important to record a sufficient number of photons without saturating the detector. We recommend recording a minimum intensity peak of 10^4 photons per field of view.

Another important point is that the phototoxicity during acquisition is lower when the laser pulse frequency is decreased. With classical Time Correlated Single Photon Counting (TCSPC) it is very important to have a count rate between 1 and 5% of the excitation rate (for 20MHz

SUPP FIGURE 1

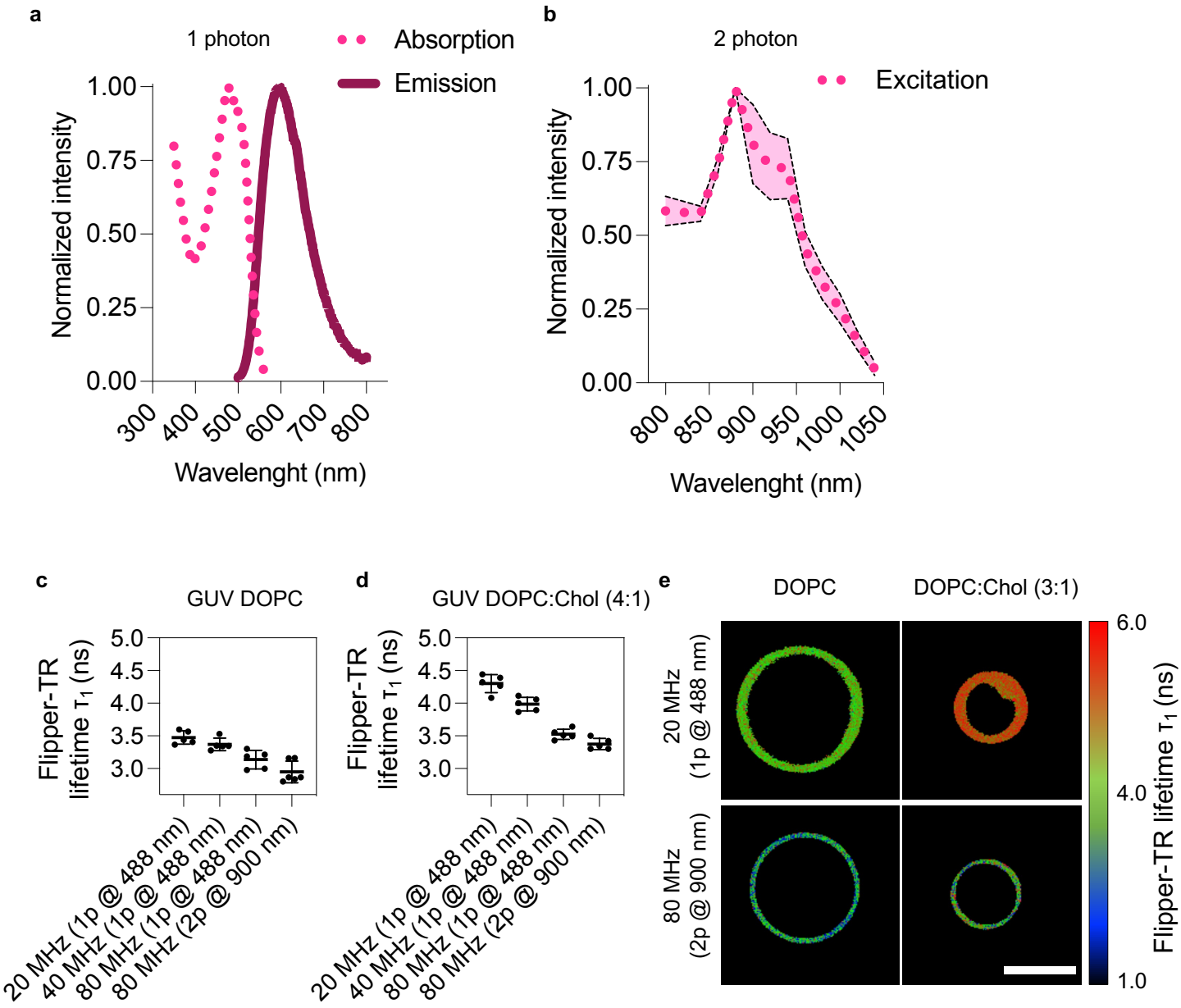

Figure S1: FLIM of Flipper-TR using two-photon microscopy

(a) Absorption and excitation spectrum of the Flipper-TR.

(b) Two-photon excitation spectra of Flipper-TR, acquired in 48h gastruloids. Five gastruloids were imaged in total at each wavelength. The acquired spectra were normalized to the maximum intensity value. Dots represented the average value, scattered lines the minimum/ maximum values of the 5 recorded spectra.

(c) and (d): Lifetime of Flipper-TR in GUVs of different compositions DOPC (c) and 1:4 DOPC:Cholesterol (d) at different laser repetition rates and under two-photon excitation. Every dot represents fitted lifetime for 1 GUV, error bars are standard deviation and line is mean.

(e) Fluorescence lifetime images of GUVs from (c,d) under typical excitation conditions (20 MHz, 488 nm, top panel) and under two-photon excitation (80 MHz, 900 nm, bottom panel). Longer lifetime component is shown (shorter lifetime component fixed). Image size is 36.4*36.4 μm^2

240 pulse, average detector count rate should not exceed 1 MHz) in order to maintain a low
241 probability of registering more than one photon per excitation cycle (with the dead time, the
242 system would detect the first photon and miss the second one, called "pile up" effect).
243 Other classic confocal microscopy parameters that participate in light acquisition (pinhole
244 aperture, laser power, pixel binning, scanning speed, size of the ROI, line averaging or
245 summation) may be used to optimize photon collection. Several means can be used to reduce
246 the phototoxicity:
247 - Using a new generation of TCSPC device with reduced dead time (rapidFLIM from
248 Picoquant, dead time of less than 650 ps compare to 80 ns in normal FLIM) that allows to
249 detect more than one photon per excitation cycle. It also provides a better temporal resolution
250 (see below) and allows to work with higher intensities. Overall, with this new kind of TCSPC
251 much higher detector count rates can be processed while achieving better timing precision and
252 faster acquisition. This system also allows to acquire more than one photon per laser pulse
253 without the pile up effect.
254 - Repeating acquisition and summing-up photons from several images will allow to
255 obtain sufficient counts of photons (minimum peak of 10^4 events) for a reliable fit. For standard
256 cells in culture, we used the following conditions. For example, using Flipper-TR in HeLa
257 Kyoto, we could sum up to 7 frames in a 256x256 pixel image to reach 10^5 photons peak in
258 case of an entire field of view which was necessary for fitting procedure and lifetime extraction.
259 Cell type and signal intensity determine the optimal acquisition parameters. It is necessary to
260 find a reasonable balance between photon number and phototoxicity and we created a
261 troubleshooting table based on our experience (Fig 4).
262
263 Timelapse of Flipper-TR
264 Since the Flipper-TR probe is in dynamic exchange with the environment, measuring lifetime
265 over time has its own challenges. If medium is added (osmotic shocks or drug addition), we
266 advise to keep Flipper-TR concentration constant. If medium is flowed (to test the effect of
267 shear stress for example) it is essential to keep the Flipper-TR concentration constant. Because
268 lifetime values are broad due to inherent biological variability and impacted by cell density or
269 cell type, we suggest assessing both lifetime variation and absolute lifetime values.
270
271 Combining Flipper probes with drug treatment
272 To measure the effect of a drug treatment on cells, we tested two strategies. (1) Imaging the
273 cells, adding the drug in the medium of a dish or replacing the medium with the one that

FIGURE 4

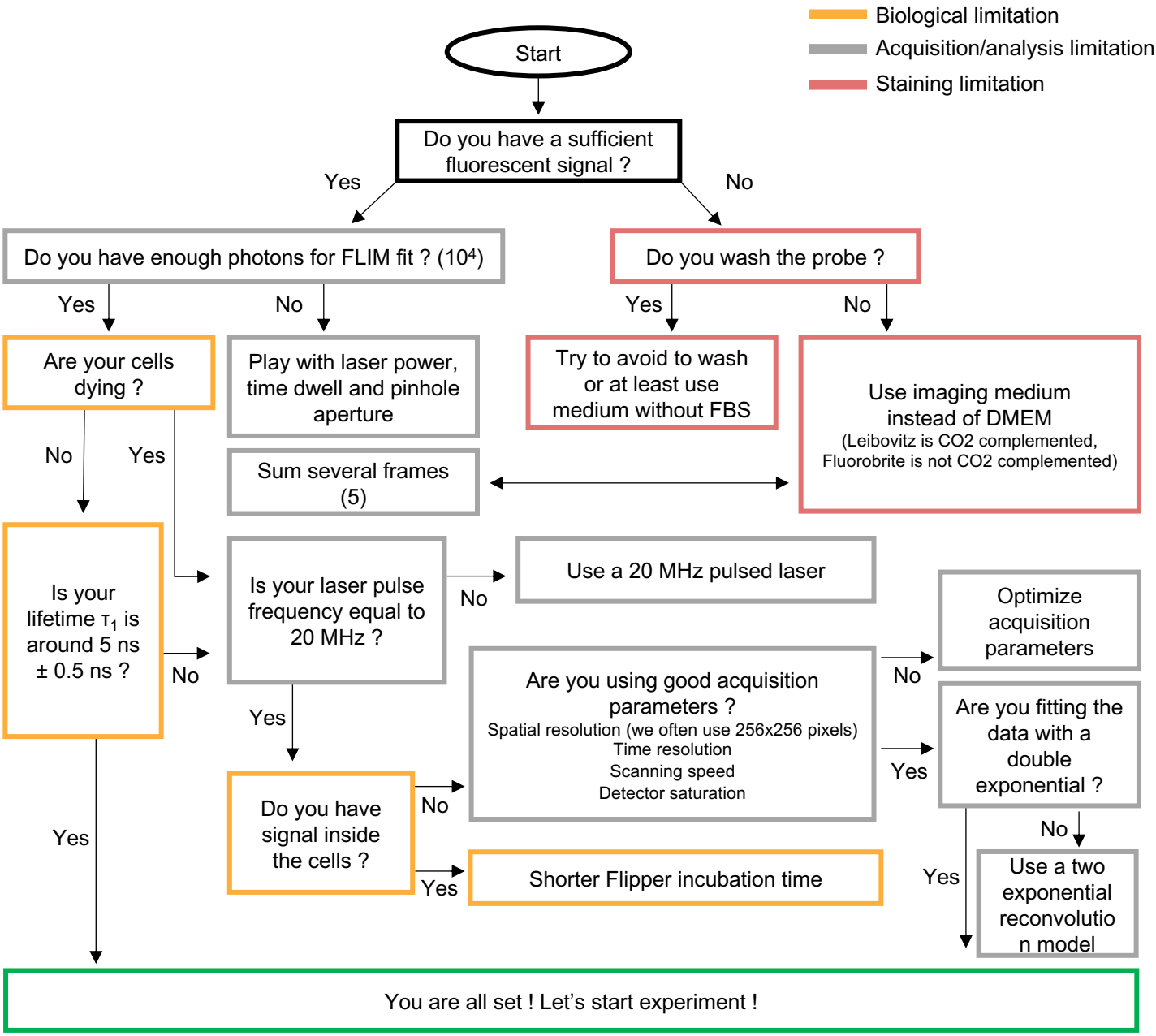

Figure 4: Chart to support users with troubleshooting Flipper probes experiments.

contains the drug using a microfluidic device and following the effect of the drug over time on the same cells. This approach allows to eliminate the biological variability by measuring the tension of the same cells before and after the treatment. (2) Imaging the control condition and the treated condition independently (preferably acquire a large amount of cells to increase statistics as it will be unpaired measurements, typically at least 15 fields of view per dish and 3 technical replicates). The treated cells must be imaged in the same conditions and on the same day. Because steady state lifetime value can be variable (it depends on cell density), the control condition must be repeated along every drug condition with the same seeding parameters. We suggest following strategy (1) whenever possible. Classical solvents (DMSO) or antibiotics used in inducible systems (doxycyclin) change the property of the membrane and therefore affect the Flipper-TR lifetime. Indeed, DMSO increases solution hypertonicity while doxycyclin affects cholesterol amounts.

<u>Acquiring lifetime in a z-stack (such as in polarized tissue)</u>

We observed a weak staining in very dense and polarized tissue independently of the incubation time (from 5 min to 2h). Tissues are not perfectly flat leading to smaller collection of photons at the apical side, which might lead to inhomogeneous signal and thus poorly reproducible results. To compare lifetime of the Flipper-TR along Z-axis, samples and conditions, we suggest defining the basal or mid-plane as the plane with the largest number of photons. Due to the inherent difficulty to measure the lifetime of single cells, we advise to compare planes containing several cells.

III-Analysis

A-Tools to analyse the data

Several companies have made commercial packages for FLIM analysis, but these are closed source tools that are not transparent in their analyses and typically only support their own file formats. Open source and user friendly tools have been and are being developed[21,22].

B-IRF (instrument response function)

In order to fit the signal, the contribution of instrumentation must be isolated. The overall timing precision of a complete TCSPC system is its Instrument Response Function (IRF). The best way to measure the IRF of the system is to use a fluorophore with similar fluorescence

properties as the Flipper-TR but with a very short lifetime. The IRF can be measured using fluorescein solution quenched with potassium iodide before each experiment or can be calculated (deducted) from the rising edge of the TCSPC histogram. The important point is to use the same IRF throughout the experiment. Software used to analyse FLIM images usually recalculate the IRF for each file by default.

C-Photon count fitting

Two different methods to fit the exponential decay exist: exponential reconvolution and exponential tailfit. A tailfit can be used when the lifetimes are significantly longer than the IRF. In general, a reconvolution fit is preferable, because the complete decay is fitted, while the start of the fitting range is slightly arbitrary for a tailfit. Depending on the format of the data and the available tools, choosing one or the other should not impact measurements too much if enough photons are acquired. Tens of thousands of photons per pixel are required to accurately fit a bi-exponential decay [23]. In general, lifetime histograms of Flippers are not well fitted by a mono-exponential model, so it is standard to fit the data with double exponentials. By fitting with a bi-exponential decay, two lifetimes will be extracted: τ_1 and τ_2. τ_{AVG} is an average between the two rates τ_1 and τ_2 weighted by the number of photons fitted by each parameter. τ_1 (the longest component) or τ_{AVG} will usually represent much higher photon counts than τ_2. Both τ_1 or τ_{AVG} will directly report the mechanical property of the probe so you should anyway take either τ_{AVG} or the longest τ (τ_1 on picoquant system) value to analyse tension fluctuations. In experiments analyzing the dynamics of Flipper, if the tendency of τ_1 and τ_{AVG} are different, probably because of a lack of photons, the fit and image acquisition must be optimized. In some cases, fit free approaches can be used as well. The fast lifetime (often defined as the arithmetic mean on the photon arrival times per pixel) can be used and shows similar values to the fitted average lifetime τ_{AVG}.

The exponential fitting can be done on a different set of pixels. The choice depends on the quality of your signal and the sensitivity of the effect you are looking at. (1) Whole photons analysis is the simplest and necessitate little requirement of input from the experimentalist, therefore increasing the reproducibility of the work. (2) It is possible in order to remove the background to apply a threshold on pixel intensity and only fit the corresponding pixels. It is however invalid to apply a threshold based on the lifetime values to extract lifetime. (2') Applying a threshold on the absolute lifetime value can be valid to create masks and separate

SUPP FIGURE 2

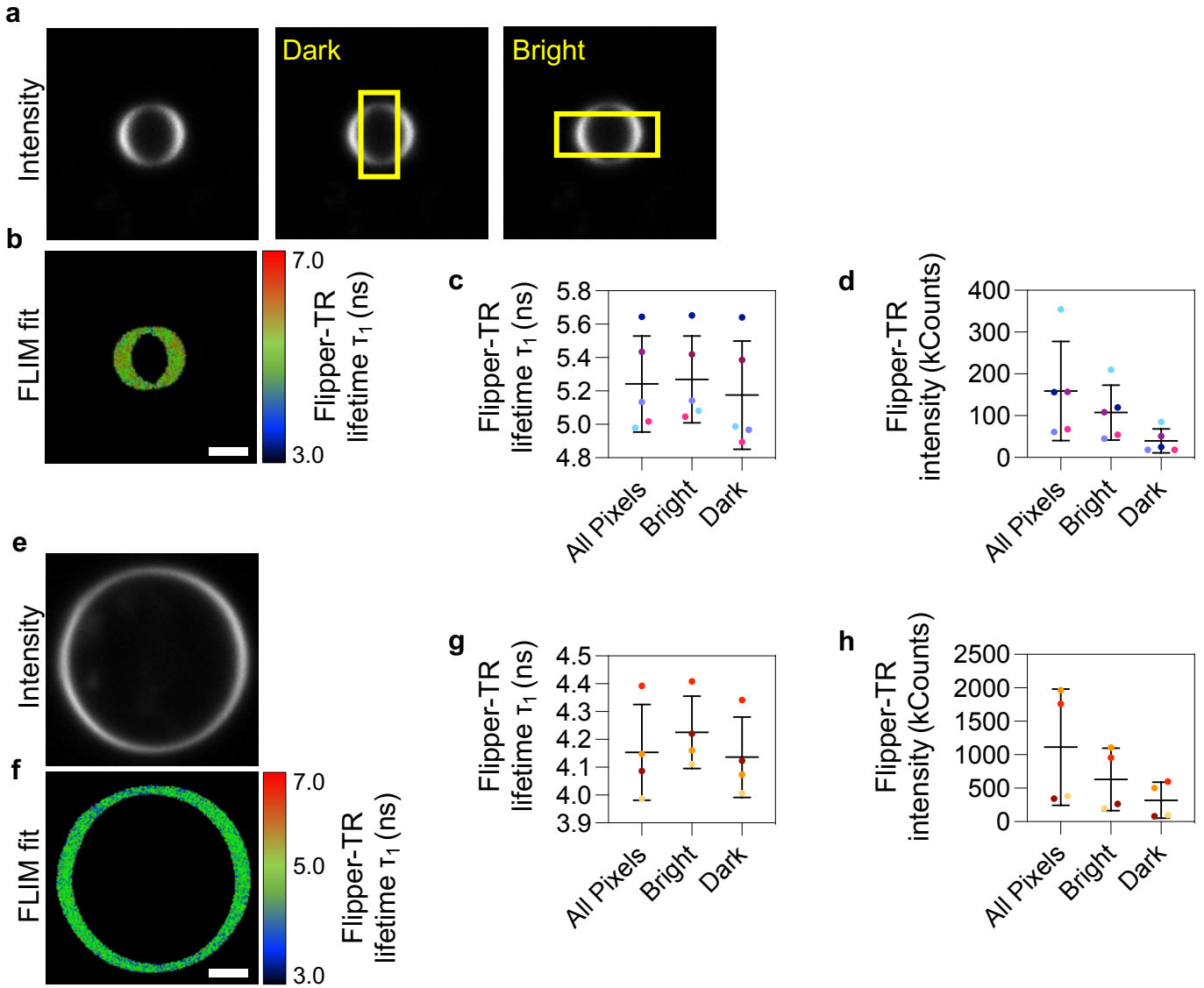

Figure S2: Effect of linearly polarised excitation light on Flipper-TR lifetime measurements in GPMVs and GUVs.

(a) Intensity and (b) Lifetime images of cell-derived vesicles. Photoselection of the fixed excitation dipole of the Flipper-TR probe (using a linearly polarized excitation laser) causes bright rings with higher intensity. Graphs show (c) Lifetime and (d) intensity analysis of bright vs dark regions. Every dot represents the lifetime fit across one vesicle. The line represents the mean and error bars are standard deviation.

(e) Intensity and (f) lifetime and image of artificial vesicle composed of DOPC and Cholesterol (4:1). Image size is 36.4*36.4 μm^2. The graphs represent (g) lifetime and (h) intensity analysis of bright vs dark regions. Every dot represents the lifetime fit across one vesicle. The line represents the mean and error bars are standard deviation.

341 objects with different Flipper lifetimes. For example, the lifetime of the plasma membrane is
342 much higher than the lifetime of endosomal membrane, so a single FLIM image could be
343 sufficient to discriminate the two objects. (3) Similar to (2), it is possible to overlap a mask
344 generated from another channel to only select pixels of interest (Fig 5a-b).
345 Depending on the orientation of the cells in the beam, the number of photons can change (Fig
346 S2). A side acquisition will give a lower number of photons than an acquisition from the
347 bottom, leading to a worse fit (Fig 5c-e). As can be noticed from the intensity images and
348 quantification (Fig S2 a, e, d, h), Flipper-TR undergoes photoselection when excited with
349 linearly polarized light. This effect can be misleading for probes like Laurdan that use
350 fluorescence intensity to report on membrane properties[24]. While the photoselection during
351 excitation can lead to bright edges of vesicles or membranes aligning or misaligning with the
352 polarization, fluorescence lifetime measurements and fitting (given enough photons are
353 acquired) is not significantly different between bright and dark regions (FigS2 c, g) and can
354 robustly report on the membrane properties. Note that the effect is stronger for membranes with
355 higher viscosity (larger cholesterol content). However, the photoselection effect can be
356 misleading when using intensity-weighted lifetime representations (as in FastFLIM).
357
358

359 D- Image segmentation to extract Flipper lifetime

360
361 Here, we will develop two examples to illustrate the importance of extracting the lifetime
362 properly. Fluorescence intensity images of a membrane probe (CellMask Deep Red for
363 instance) can be used to generate a mask that permits to extract lifetime of all the pixels present
364 in the mask (Fig 5a). Even if the lifetime of the internalized probe is lower than the lifetime of
365 the probe at the plasma membrane, applying a threshold based on lifetime value will introduce
366 a bias in the analysis of the overall lifetime. Considering only pixels corresponding to the
367 plasma membrane instead of all the pixels of the image, which include signal coming from
368 endosomes, gives a difference of 0.5 ns on average (Fig 5b).
369 The second example is illustrated by measuring the impact of blebbistatin (myosin inhibitor
370 reducing cell contractility) on plasma membrane tension reported by Flipper-TR lifetime (Fig
371 5f). If all the pixels of the images (control versus blebbistatin-treated cells) are included for the
372 fitting, a decrease of lifetime of 0.3 ns is observed (Fig 5g). Each dots represent a field of view
373 containing several cells, the fitting was performed by fitting all the pixels. However, it appears
374 that on images of Blebbistatin-treated cells, despite an identical Flipper-TR incubation time,

FIGURE 5

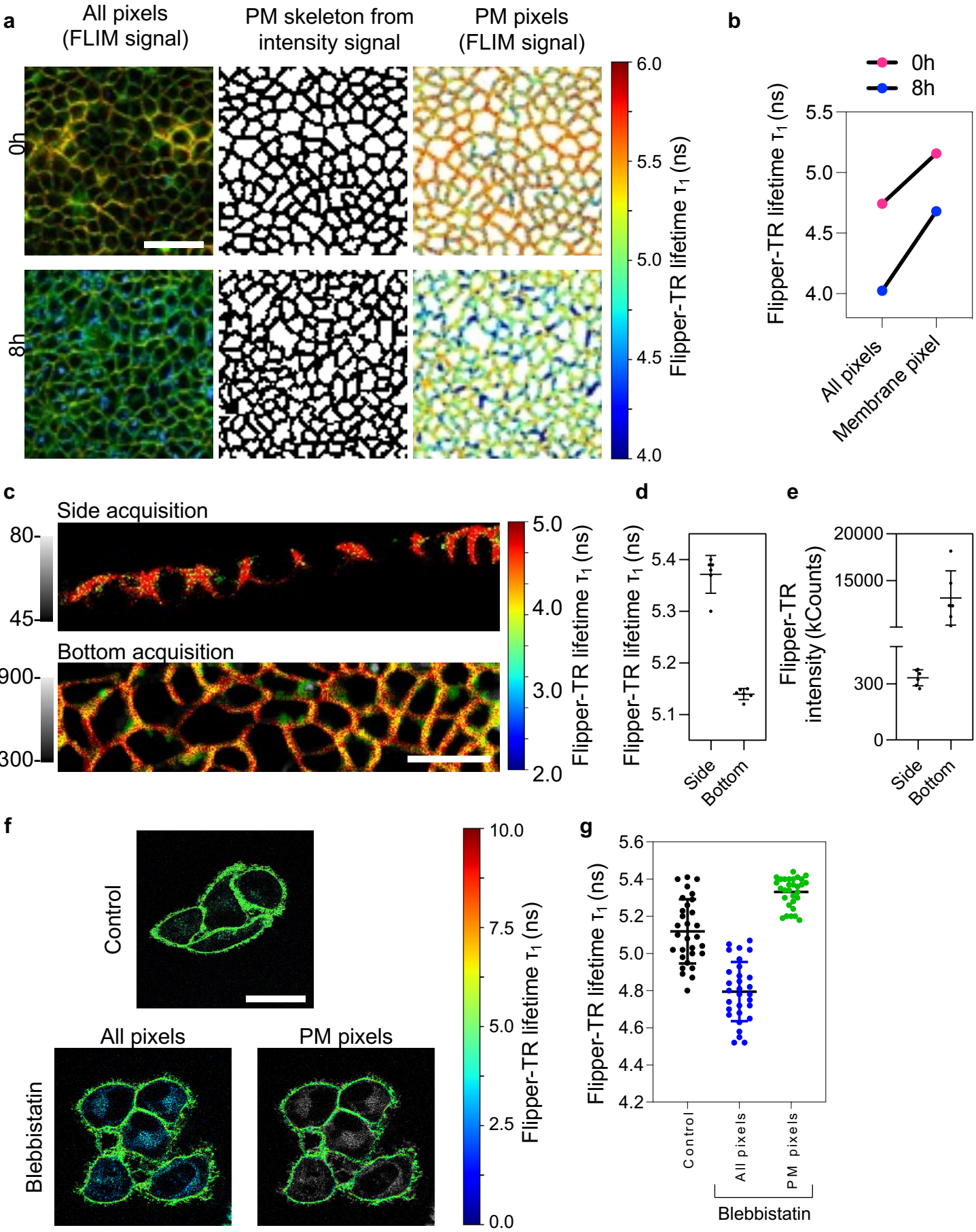
a
All pixels (FLIM signal)
PM skeleton from intensity signal
PM pixels (FLIM signal)
0h
8h
6.0
5.5
5.0
4.5
4.0
Flipper-TR lifetime τ1 (ns)
b
0h
8h
Flipper-TR lifetime τ1 (ns)
5.5
5.0
4.5
4.0
All pixels
Membrane pixel
c
Side acquisition
80
45
Bottom acquisition
900
300
5.0
4.0
3.0
2.0
Flipper-TR lifetime τ1 (ns)
d
Flipper-TR lifetime τ1 (ns)
5.4
5.3
5.2
5.1
Side
Bottom
e
Flipper-TR intensity (kCounts)
20000
15000
300
0
Side
Bottom
f
Control
All pixels
PM pixels
Blebbistatin
10.0
7.5
5.0
2.5
0.0
Flipper-TR lifetime τ1 (ns)
g
Flipper-TR lifetime τ1 (ns)
5.6
5.4
5.2
5.0
4.8
4.6
4.4
4.2
Control
All pixels
PM pixels
Blebbistatin

Figure 5: How to properly extract the Flipper-TR lifetime from FLIM image.

(a) Representative FLIM images of MDCK tissue stained with Flipper-TR (top row) with and without endosomal staining (respectively top panel and bottom panel after 8h of incubation) due to longer cell incubation with Flipper-TR. Flipper-TR lifetime of pixels corresponding only to plasma membrane (PM) extracted via the segmentation of the PM (middle column) based on Flipper-TR fluorescence intensity.

(b) Graph showing the Flipper-TR lifetime (τ_1, ns) extracted from all the pixels of the image versus only the pixels corresponding to the plasma membrane.

(c) Representative FLIM images of MDCK tissue stained with Flipper-TR acquired from the side (top row) or from the bottom (bottom row).

(d) Graph showing the Flipper-TR lifetime (τ_1, ns) extracted from the pixels of the side acquisition image versus from the bottom acquisition image.

(e) Graph showing the number of photons extracted from the pixels of the side acquisition image versus from the bottom acquisition image.

(f) Representative FLIM images of HeLa cells incubated with DMSO (top) or with blebbistatin (bottom). Bottom images show two configurations: all the pixels are selected (left) or only pixels corresponding to PM were manually selected (right). Scale bar is 40 μm.

(g) Graph showing Flipper-TR lifetime quantification corresponding to (c). Lifetime (τ_1, ns) was extracted from all the pixels of the image versus only the pixels corresponding to the plasma membrane (n=30 for both control and blebbistatin treated cells)

375 many intracellular membranes with a low lifetime around 2.5 ns are visible. These pixels likely
376 contribute to the overall lower lifetime measured for Blebbistatin-treated cells. By contrast, if
377 only plasma membrane lifetime is measured, by selecting the plasma membrane pixels, the
378 average lifetime of Blebbistatin-treated cells is 0.1 ns higher than the average lifetime of control
379 cells. Directly selecting the plasma membrane pixels also excludes the background, which
380 could affect the analysis.
381

382 E-Comparing different areas within the same image

383
384 The goal of the experiments might be to compare regions within the same image. As explained
385 above, a minimum number of photons will be necessary to obtain a decent fit and to extract the
386 lifetime properly. Therefore, we strongly suggest to check that the photon count is similar
387 between different area analyzed.
388

389 IV-Results

390

391 A-Different lifetime along cell height

392
393 By imaging Flipper-TR over z-stacks of MDCK polarized tissues, we observed a lower lifetime
394 (4.6 ns) at the basal plane of the cell compared to the apical plane (5.4 ns), as illustrated in Fig
395 6a. Also, large variability exists between position in the dish: the basal plane lifetime values
396 vary from 4.2 ns to 5.1 ns, while the apical plane values vary between 4.3 ns and 5.6 ns.
397 However, the lifetime in the apical plan is reproducibly higher than in the basal plan (Fig 6b)
398 which could be explained by the known differences in lipid compositions. Therefore, single
399 plane imaging of cells to compare, for example, different treatments, must be performed at a
400 similar height (Fig 6c), and sufficient statistics to account for large biological differences
401 between single cells are required.
402

403 B-Mitotic cells have a more disordered plasma membrane

404
405 We analyzed the Flipper-TR lifetime in mitotic cells which are known to have a higher volume,
406 higher cortical tension and a very different shape than adherent cells[25–27]. Mitotic cells were
407 identified by eye based on their rounded shape and their limited attached surface to the glass
408 bottom. In contrast to the literature, mitotic cells have a 0.35 ns lower lifetime (Fig 6d)

FIGURE 6

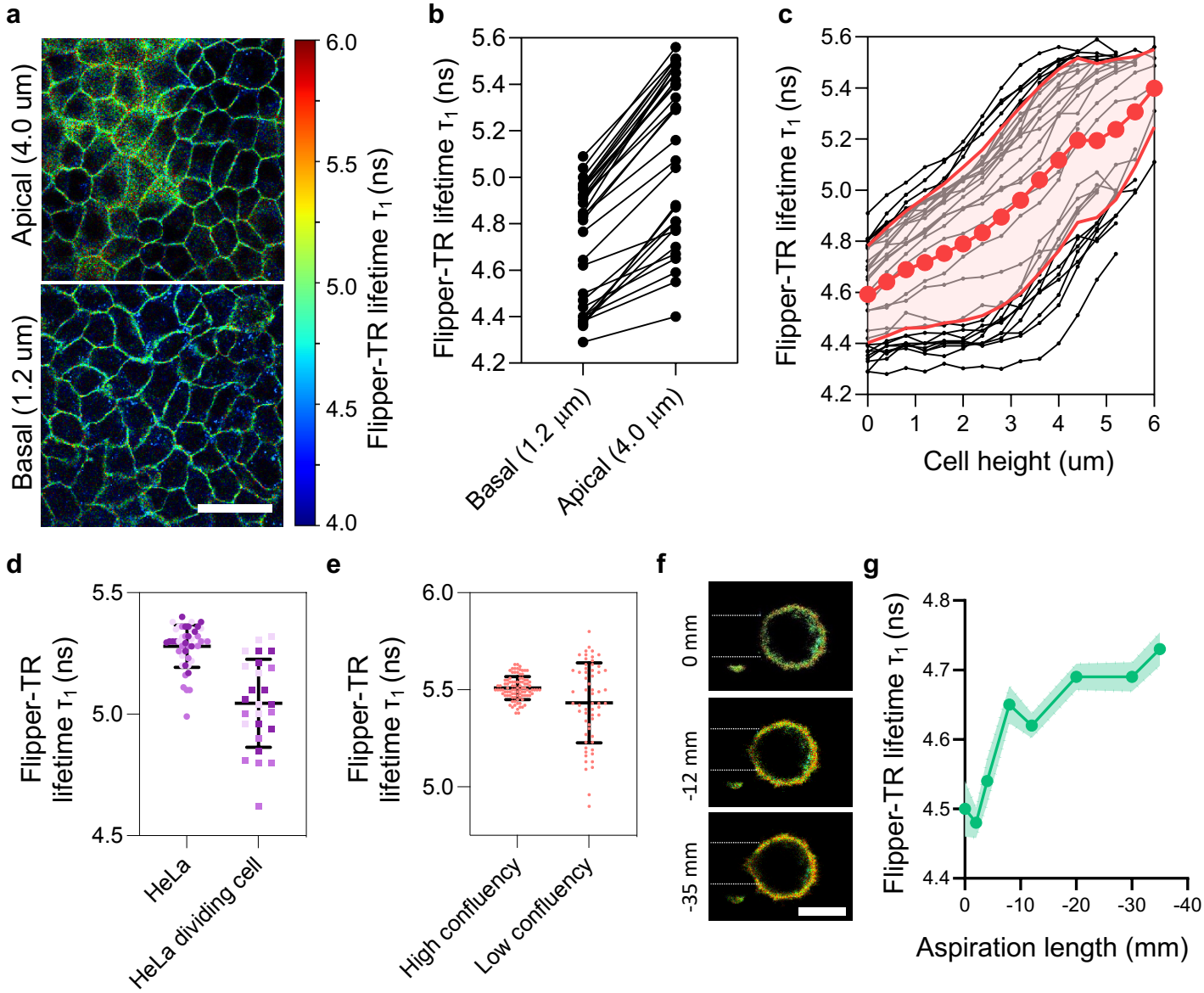
a
Apical (4.0 um)
Basal (1.2 um)
6.0
5.5
5.0
4.5
4.0
Flipper-TR lifetime τ1 (ns)
b
Flipper-TR lifetime τ1 (ns)
5.6
5.4
5.2
5.0
4.8
4.6
4.4
4.2
Basal (1.2 µm)
Apical (4.0 µm)
c
Flipper-TR lifetime τ1 (ns)
5.6
5.4
5.2
5.0
4.8
4.6
4.4
4.2
0
1
2
3
4
5
6
Cell height (um)
d
Flipper-TR lifetime τ1 (ns)
5.5
5.0
4.5
HeLa
HeLa dividing cell
e
Flipper-TR lifetime τ1 (ns)
6.0
5.5
5.0
High confluency
Low confluency
f
0 mm
-12 mm
-35 mm
g
Flipper-TR lifetime τ1 (ns)
4.8
4.7
4.6
4.5
4.4
0
-10
-20
-30
-40
Aspiration length (mm)

Figure 6: Flipper-TR lifetime is affected by several parameters

(a) Representative FLIM images of MDCK tissue stained with Flipper-TR in the apical plan (top row) ant the basal plan (bottom row). Scale bar is 40 µm.

(b) Graph showing the quantification of Flipper-TR lifetime (ns) in the apical plane (4.0 micron from the bottom) and the basal plane (1.2 micron from the bottom). The bottom was determined as the plane with the highest number of photons (n = 45).

(c) Graph showing the quantification of Flipper-TR lifetime (τ_1, ns) from the bottom plane to the apical plane by steps of 0.4 micron. Each curve represents the lifetime of an entire field of view (n = 45).

(d) Graph showing the quantification of Flipper-TR lifetime (τ_1, ns) in mitotic and non-mitotic HeLa cells

(e) Graph showing the quantification of Flipper-TR lifetime ($\tau 1$, ns) in confluent and non-confluent RPE1 cells

(f) Representative Flipper-TR FLIM images of HeLa cell aspirated in a micropipette at different aspiration pressure. Scale bar: 10 µm

(g) Graph showing the quantification corresponding to (c) of Flipper-TR lifetime (τ_1, ns) depending on the aspiration pressure applied to the cell.

409 compared to adherent cells[26,27], while one might have expected an increase of Flipper-TR
410 lifetime. This lower lifetime could reflect a change of lipid composition during cell division[28],
411 itself causing increased membrane fluidity in mitotic cells[29].
412

413 C- Flipper-TR variability depends on cell confluency

414
415 We analyzed the Flipper-TR lifetime depending on cell confluency. Using RPE1 cells, we
416 observed that confluent cells have a Flipper-TR lifetime centered around 5.5 +/- 0.1 ns while
417 non-confluent cells lifetime is centered around 5.4 +/- 0.2 ns (Fig. 6e). Therefore, in case of
418 experiments performed using cells at low confluency, larger statistics are required to account
419 for large biological differences between single cells.
420

421 D- Distinguishing the contributions of lipid composition and tension to the
422 changes of lifetime

423
424 Previous work from the lab[8] showed that mechanical increase of Giant Unilamellar Vesicles
425 (GUVs) membrane tension induced by micropipette aspiration (high tension) leads to an
426 increase of 0.2 ns of Flipper-TR lifetime. Using the same setup to aspirate HeLa cells in
427 suspension (Fig 6f), an increase of 0.2 ns was also observed (Fig 6g), confirming that in both
428 GUVs and cells Flipper-TR lifetime measurements can directly report a mechanically induced
429 change of membrane tension.
430 Although being slightly lower than Flipper (steady state lifetime of 5 ns vs 5.8 ns for SM/Chol
431 GUV), the lifetime of super-resolution (SR)-Flipper also reports changes in membrane tension
432 of GUVs (Fig 7a-b) as well as change in lipid packing (composition). Indeed, SR-Flipper-TR
433 lifetime of SM/Chol (70/30) GUV is centred around 5 ns while the lifetime of DOPC/Chol
434 (70/30) GUV is centred around 4.2 ns (Fig 7b). With both lipid compositions, SR-Flipper
435 lifetime decreases upon membrane tension decrease induced by hypertonic shocks proving that
436 Flipper probes lifetime report both lipid composition and membrane tension (Fig 7a-e). In
437 contrast, the lifetime of pure DOPC GUVs is not changing after hypertonic shock which is in
438 good agreement with an absence of phase separation (Fig 7a,f).
439 Niemann-Pick C1 protein (NPC1) is responsible of the intracellular transport of Cholesterol
440 and sphingolipids. Consequently, the depletion of NPC1 is responsible for cholesterol
441 accumulation in endosomes. Consistently, LysoFlipper in HeLa MZ NPC1 KO cells have a
442 higher lifetime than in WT HeLa cells indicating higher lipid packing (Fig 7g-h). Nonetheless,

FIGURE 7

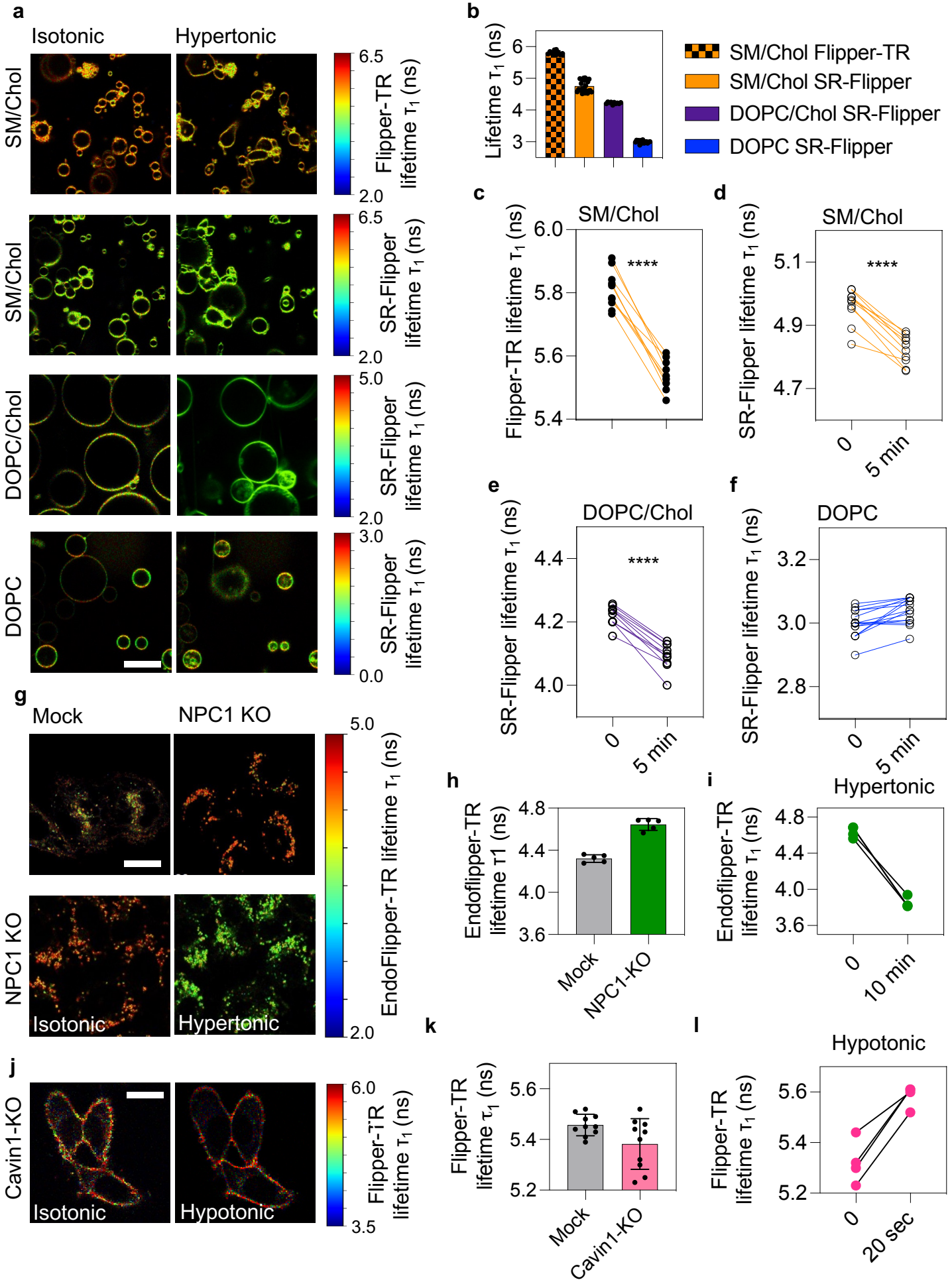
a
Isotonic
Hypertonic
SM/Chol
SM/Chol
DOPC/Chol
DOPC
Flipper-TR lifetime τ1 (ns)
SR-Flipper lifetime τ1 (ns)
6.5
2.0
5.0
3.0
0.0
b
Lifetime τ1 (ns)
SM/Chol Flipper-TR
SM/Chol SR-Flipper
DOPC/Chol SR-Flipper
DOPC SR-Flipper
c
SM/Chol
Flipper-TR lifetime τ1 (ns)
****
d
SM/Chol
SR-Flipper lifetime τ1 (ns)
0
5 min
e
DOPC/Chol
f
DOPC
g
Mock
NPC1 KO
Isotonic
Hypertonic
EndoFlipper-TR lifetime τ1 (ns)
h
Endoflipper-TR lifetime τ1 (ns)
Mock
NPC1-KO
i
Hypertonic
10 min
j
Cavin1-KO
Hypotonic
k
l
20 sec

Figure 7: Flipper lifetime allow to detect membrane tension variations although if lipid composition is different.

(a) Representative FLIM images before and after hypertonic shocks of SM/Chol containing GUVs stained with Flipper-TR or SR-Flipper, DOPC/Chol containing GUVs stained with SR-Flipper and of DOPC containing GUVs stained with SR-Flipper (d).

(b) Graph showing the quantification of Flipper-TR and SR-Flipper lifetime (τ_1, ns) before hypertonic shock on GUV of specified lipid composition.

(c) Graph showing the quantification of Flipper-TR lifetime (τ_1, ns) before and after hypertonic shock on SM/Chol GUV.

(d-f) Graph showing the quantification of SR-Flipper lifetime (τ_1, ns) before and after hypertonic shock on GUV of specified lipid composition.

(g) Top : representative Endo Flipper FLIM images of HeLa MZ cells (left) and HeLa MZ NPC1 KO cells (right), which present accumulation of Cholesterol in endosomes. Bottom : representative Endo Flipper FLIM images of HeLa MZ NPC1 KO cells before hypertonic shock (left) and after hypertonic shock (right).

(h) Graph showing the quantification of Endo Flipper lifetime (ns) of HeLa MZ cells and HeLa MZ NPC1 KO cells

(i) Graph showing the quantification of Endo Flipper lifetime (τ_1, ns) before and after hypertonic shock

(j) Representative Flipper-TR FLIM images of HeLa Cavin1-KO cells before hypotonic shock (left) and after hypotonic shock (right).

(j) Graph showing the quantification of Flipper-TR lifetime (τ_1, ns) in HeLa cells (n = 10) and HeLa Cavin1-KO cells (n = 10) in isotonic medium.

(k) Graph showing the quantification of Flipper-TR lifetime (τ_1, ns) in HeLa Cavin1-KO cells (n = 4) after a hypotonic shock

the probe is still able to report a change in membrane tension, as demonstrated by lifetime decrease under hypertonic treatment (Fig 7g,i).

The protein Cavin1 is a major component of caveolae and its deletion prevents caveolae assembly[10,30]. Interestingly, the absence of caveolae is associated with a smaller Flipper-TR lifetime, indicating either a lower membrane tension or a more disordered membrane composition (Fig 7j-k). Cavin1-KO cells show a lifetime increase upon hypotonic shocks (Fig 7j,i). Despite a potential difference of lipid composition, Flipper-TR is anyway able to report an increase of membrane tension.

Conclusion:

Here, we have reported the current technical difficulties we faced using Flipper probes, and how we overcame them. In the future, further developments of Flipper probes will allow us to bypass some of these problems. Technical improvements in the FLIM image acquisition and analysis may also help spread the use of Flipper probes to all biological samples of interest. Flipper probes remain an interesting tool for many applications, and in some cases, the only available tool to measure membrane tension.

Acknowledgment

We thank Shankar Srinivas and Christophe Royer (University of Oxford) for isolating and staining the mouse embryos. FS is grateful for the support from the EMBO (ALTF 849-2020) and HFSP (LT000404/2021-L) long-term postdoctoral fellowships. FS thanks Scott Fraser (University of Southern California) for the support and supervision and acknowledges the Translational Imaging Center (University of Southern California) for access to instrumentation and expertise. A.C. also acknowledges funding from MCIU, PID2019-111096GA-I00; MCIU/AEI/FEDER MINECOG19/P66, RYC2018-024686-I, and Basque Government T1270-19. VD thanks Pierre-François Lenne (IBDM Marseille) for supervision and resources, and Katia Barrett for preparation of Xenopus explants. V.D. acknowledges support by an HFSP long-term postdoctoral fellowship (HFSP LT0058/2022-L) and the France-BioImaging infrastructure supported by the French National Research Agency (ANR–10–INBS- 04-01, Investments for the future). VD thanks Frank Schnorrer (IBDM Marseille) for access to the FLIM system. SM thank the University of Geneva, the National Centre of Competence in Research (NCCR) Chemical Biology (51NF40-185898), the NCCR Molecular Systems Engineering (51NF40-182895), and the Swiss NSF (Excellence Grant 200020 204175; SNSF-ERC Advanced Grant TIMEUP, TMAG-2_209190) for financial support. AR acknowledges funding from the Swiss National Fund for Research Grants N°310030_200793 and N°CRSII5_189996, the European Research Council Synergy Grant N° 951324 R2-TENSION.

460 **Materials and Methods**

461

462 **Cell culture**

463 HeLa-MZ cells (Lucas Pelkmans, University of Zurich), HeLa MZ-NPC1 KO cells, HeLa-
464 Kyoto-smURFP, HeLa-Kyoto cells from Cell Lines Service (CLS) (330919) and Madin-Darby
465 Canine Kidney II (MDCK-II) (ECACC, Cat. No. 00062107) were cultured in Dulbecco's
466 modified Eagle medium (DMEM 61965026, Thermo Fisher Scientific, Waltham, USA)
467 supplemented with 10% fetal bovine serum (FBS 102701036, Thermo Fisher Scientific), 1%
468 penicillin-streptomycin (15140122, Thermo Fisher Scientific) and 1% non-essential amino
469 acids solution (NEAA 11140035, Thermo Fisher Scientific), at 37°C and 5% CO_2. Cells were
470 regularly tested negative for contamination with mycoplasma (Eurofins GATC Biotech,
471 Konstanz, Germany). The HeLa ATCC Cavin1-KO cell line and corresponding control were
472 cultured in DMEM, 4.5 g/L glucose supplemented in pyruvate. MDA MB 431 cells were
473 maintained as described von Schwedler, U. K. et al. The protein network of HIV budding. Cell.
474 The keratinocytes were grown in Keratinocyte-SF growth medium (INVITROGEN,
475 17005042) supplemented with 50 mg/mL bovine pituitary extract (BPE; Gibco) and 5 ng/mL
476 prequalified human recombinant epidermal growth factor 1-53 (EGF 1-53; Gibco).
477 Hippocampal neurons were grown in neuro basal medium. A549 and A596 were grown in
478 RPMI 1640 Glutamax Medium (INVITROGEN 61870010). All cell media were supplemented
479 with 10% foetal bovine serum (10270-106; Thermofischer) and 1% penicillin-streptomycin in
480 a 5% CO_2 incubator. Our HeLa-MZ cells were authenticated by Microsynth (Balgach,
481 Switzerland), which revealed 100% identity to the DNA profile of the cell line HeLa (ATCC:
482 CCL-2) and 100% identity over all 15 autosomal short tandem repeats (STRs) to Microsynth's
483 reference DNA profile of HeLa. Our cell lines are not on the list of commonly misidentified
484 cell lines maintained by the International Cell Line Authentication Committee. Cells were
485 authenticated by Microsynth (Balgach, Switzerland) and are mycoplasma negative, as tested
486 by GATC Biotech (Konstanz, Germany), and are not on the list of commonly misidentified
487 cell lines maintained by the International Cell Line Authentication Committee. A.Thaliana
488 embryon was deposited inside a 2ml Eppendorf that contained a solution of 500ul of water with
489 2uM Flipper-TR final concentration and incubated 45 min at RT. Embryos were immobilized
490 with 0.5% of low melting point agar for imaging. Alginate capsules and alginate tubes
491 techniques were described respectively in [31]and [32].

492

493 **Reagents and drugs treatment**

494 We obtained EZ-Link Sulfo-NHS-SS-Biotin, from Thermo Fisher Scientific. We obtained
495 DOPC, DSPE-PEG-Biotin, DOPE, DOPS and lissamine rhodamine B sulfonyl (18:1) Rhod PE
496 from Avanti Polar Lipids (Alabaster, AL). We obtained the different Flipper probes from
497 Spirochrome (SC020) or from the lab of Prof. Stefan Matile. For the experiments involving
498 blebbistatin, the concentrations of blebbistatin (SIGMA B0560-5MG) was equal to 10 uM and
499 kept constant throughout the experiment. Cells were preincubated in DMEM with blebbistatin
500 at 37 °C for 45 min. DMEM was replaced by Leibovitz with blebbistatin and Flipper-TR for
501 15 min. Blebbistatin was diluted in DMSO. Other reagents and chemicals were obtained from
502 Sigma-Aldrich (St. Louis, MO).

503

504 **Live-cell FLIM imaging**

505 For FLIM imaging, cells were seeded into 35mm MatTek glass bottom microwell dishes
506 (MatTek Corporation). Cells were rinsed with 1ml Leibovitz's medium (Thermofischer,
507 21083027) supplemented with 10% Foetal Bovine Serum and 1% Penicillin Streptomycin or
508 Fluorobrite DMEM imaging medium (Life Technologies, Thermofisher) and incubated 15 min
509 at 37°C with 1 μM Flipper (same concentration and incubation time for all Flippers). FLIM
510 imaging was performed using a Nikon Eclipse Ti A1R microscope equipped with a Time
511 Correlated Single-Photon Counting (TCSPC) module from PicoQuant. Excitation was
512 performed using a pulsed 485nm laser (PicoQuant, LDH-D-C-485) operating at 20 MHz, and
513 emission signal was collected through a bandpass 600/50nm filter using a gated PMA hybrid
514 40 detector or a TimeHarp 260 PICO implemented board (PicoQuant). For analysis, the
515 SymPhoTime 64 software (PicoQuant) was used to fit the fluorescence decay data (from full
516 images or selected pixels depending on the experiment) to a dual exponential reconvolution
517 model, whereby the longer lifetime τ_1 was extracted. Data are expressed as the mean ± s.d.

518

519 **Giant unilamellar vesicles (GUVs) electroformation**

520 GUVs were produced as described[33] in water containing 250mM sucrose. Briefly, 20 μl of 1
521 mg/mL lipid mix (DOPC: DOPS, 6:4, mol:mol) were deposited on two indium tin oxide
522 (ITO)-coated glass slides (70-100Ω resistivity, Sigma-Aldrich) and placed in a vacuum
523 drying oven for 60' for complete solvent evaporation. An O-ring of ~1mm thickness was
524 used as a non-leaky spacer between the two ITO slides, and the chamber was formed

525 by compressing the two slides with spring metal tweezers. The formed chamber was filled
526 with 400µl of 250mM sucrose solution (osmolarity adjusted to outside buffer solution, around
527 250 mOsm) and exposed to 1V AC-current (10Hz sinusoidal) at room temperature for 1 h. The
528 resulting suspension was collected in a tube and used within the next days for experiments.
529 Here, the lipid composition used were DOPC (99, 997%) and 0.003% DSPE-PEG(2000)
530 Biotin, DOPC:Cholesterol at 70:30 Mol%, containing 0.003% DSPE-PEG(2000) Biotin or
531 Brain Sphingomyelin:Cholesterol at 70:30 Mol% containing 0.003% DSPE-PEG(2000)
532 Biotin.

533 **Hypertonic shock on GUVs labelled with Flipper or SR-Flipper**

534 One channel of multi-well flow chambers (Ibidi) with 24x60mm glass coverslips (Menzel-
535 Glaser) was coated with 0.1 mg/ml avidin in water for 10min, and rinsed 3X with water and
536 2X PBS. 2µl GUVs were added in 50µl PBS during 5min to facilitate avidin-biotin interactions,
537 and then the solution was replaced by 40µl of 0.1mg/ml albumin-biotin in buffer 1 in order to
538 saturate free avidin sites. The chamber was washed with 60µl of PBS and 1µM of specified
539 Flipper was added on GUVs. For analysis, ROIs were selected by focusing on the GUV
540 equatorial plane. For osmotic shocks, PBS was replaced with a pump at a rate = 60µl/min to
541 avoid GUV damages by PBS supplemented with 250mM sucrose (final osmolarity of 500
542 mosm) or PBS diluted 2 times with water (125 mosm). A FLIM image was recorded before
543 osmotic shock and 5min after the shock. Lifetime extraction was performed as previously
544 described.

545

546 **Hypotonic shock on HeLa ATCC Cavin1-KO labelled with Flipper-TR**

547 Cells were seeded into 35-mm MatTek glass-bottom microwell dishes. For hypotonic shocks,
548 we diluted the cell imaging media with MilliQ water. Under the microscope, 1 mL of MilliQ
549 water solution was added to the imaging dish containing 0.330 mL of isotonic buffer during
550 imaging to reach a final osmolarity of 120 mOsm. Osmotic shocks were applied 10 seconds
551 before the second timepoint.

552

553 **Micropipette aspiration on cells**

554 The experimental set-up used to aspirate cells with a micropipette was the same as previously
555 reported[33], and combines bright-field imaging, confocal scanning microscopy and FLIM
556 imaging on an inverted Nikon Eclipse Ti microscope. Approximatively 1000 HeLa Cells in

557 suspension were injected in the chamber (previously passivated with casein) containing
558 complete medium supplemented with 0.5M of sucrose (in order to have a reasonably low
559 plasma membrane tension which is necessary for pipette aspiration). A cell was aspirated by
560 setting a negative pressure on the micropipette and FLIM images were acquired at different
561 pressures. The analysis was performed as mentioned before.
562
563 **Fluorescence recovery after photobleaching (FRAP) experiments**
564 Flipper was imaged using a ×100 1.4 numerical aperture oil DIC plan-apochromat VC
565 objective (Nikon) with a Nikon A1 scanning confocal microscope. Photobleaching was
566 performed in circular regions with four iterations of 488 nm at 100% laser intensity. For the
567 analysis, the fluorescence background was subtracted from the intensity values of the ROIs.
568 Those values were subsequently normalized to an unbleached area and the value of the intensity
569 of the first frame after bleaching was subtracted. Finally, FRAP curves were normalized to the
570 value of the pre-bleach fluorescence intensity. To determine the FRAP recovery kinetics, we
571 fitted with the following double exponential function
572 $f(t) = \alpha(1 - et - t0/\tau1) + (1 - \alpha)(1 - et - t0/\tau2)$, where τ_1 and τ_2 are the time constants and α is
573 the weight fraction of the exponential with characteristic time τ_1. Diffusion coefficients were
574 extracted with the formula: $D=Rn^2+Re^2/8\tau1/2$ from[34].
575
576 **Experiments with GPMVs**
577 Giant plasma membrane vesicles (GPMVs) were produced from HEK293T cells which were
578 maintained under standard culture conditions, 37 °C, 5% CO2 with DMEM (Corning) 10 %
579 FBS, Penicillin (100 U/mL) Streptomycin (100 µg/mL) (Lonza) and 2 mM L-Glutamine
580 (Sigma Aldrich) following the procedure described previously[35,36]. Cells were seeded a day
581 prior to the GPMV production and allowed to grow to a confluence of about 75 %. To induce
582 vesiculation, growth media was removed, the cells washed once with GPMV buffer (containing
583 150 mM NaCl, 10 mM HEPES, 2 mM CaCl2 at pH 7.4), and next PFA and DTT were added
584 to a final concentration of 25 mM and 5 mM, respectively. The cells were incubated for 2.5 h
585 at 37 °C. The supernatant containing the GPMVs was harvested, and detached cells were
586 removed by a short centrifugation (90 seconds at 1000 g). GPMVs were labelled with 1 µM
587 Flipper-TR (final concentration) for 5 minutes before transfer to an imaging chamber (IBIDI
588 18well µ slide #1.5 glass). To non-specifically immobilize the GPMVs partially for imaging,

589 the cover glass was treated with poly-D-Lysine (0.1 mg/mL) for 30 minutes and washed
590 extensively with PBS as described previously[37].
591
592 **Lifetime imaging using Leica SP8 FALCON**
593 One and two photon FLIM measurements were performed at a Leica SP8 equipped with
594 FALCON and Dive modules (Leica Microsystems) and a 40x HC PL IRAPO 1.10 NA water-
595 immersion objective (Leica Microsystems). Flipper fluorescence was excited using the white
596 light laser (Leica Microsystems) with repetition rates of 80 MHz, 40 MHz, or 20 MHz and
597 emission set to 488 nm in one photon mode or fluorescence was excited at 900 nm using a
598 tunable Spectra Physics InSight X3 Ti:Saphire laser (pulsing at 80 MHz) in two photon mode.
599 Fluorescence was collected between 500 nm and 700 nm on internal HyD-SMD detectors (in
600 a descanned path for one photon and non-descanned path for two photon mode, respectively).
601 The pinhole was set to 1.2 AU (at 550 nm). Images were acquired at 700 Hz scanning frequency
602 at a zoom of 5 (512 by 512 pixels resulting in a pixel size of 113.9 nm/px). For one FLIM
603 image 25 frames were accumulated to acquire at least 10^4 photons at peak of the TCPSPC
604 curve. Laser powers were adjusted when data were recorded at different repetitions rates to
605 maintain similar count rates.
606
607 **Leica SP8 image processing**
608 Image analysis and processing were performed in LAS-X (Leica Microsystems) and FIJI[38].
609 All lifetime data were obtained by applying a tailfit either for the whole image or on per pixel
610 basis. For fitting Flipper decay data, a two-exponential model had to be employed. The shorter
611 component was fixed based on the average short lifetime (of the whole image) for one
612 respective dataset/condition (typically around 0.7 – 1.1 ns). The second component was
613 extracted after fitting again (with short lifetime fixed) and presented as the tension sensitive
614 component. In one photon mode, tail fitting was performed from 2.5 ns to 8.2 ns (80 MHz),
615 2.5 ns to 20 ns (40 MHz), or 2.5 ns 44 ns (20MHz). In two photon mode, fitting was performed
616 from 2 ns to 12 ns (80 MHz). Generally, lower fitting boundary was about 0.5 ns from TCPSC
617 maximum and on the edge of the estimated IRF. For the analysis of GUV and GPMV data,
618 images were cropped to 320 by 320 pixels (36.4 µm by 36.4 µm), binned by a factor of 2 to
619 increase photon count per pixel, and thresholded to exclude background pixels (for the
620 GPMVs). Finally, the image fit was performed keeping the short lifetime component fixed and
621 the longer component floating. Fitted lifetimes per image were exported to Excel. FLIM images
622 were exported as raw images to .tiff (using 0.001 lifetime values per gray level accuracy). For

presentation, images were thresholded using the intensity image and a rainbow LUT applied to the second lifetime component (all performed in FIJI as described previously[16]).

Fluorescence Lifetime Imaging Microscopy of gastruloids and Xenopus explants

FLIM measurements were performed on a Zeiss LSM880 system (Carl Zeiss, Oberkochen, Germany) equipped with a time-resolved LSM upgrade (PicoQuant GmbH, Berlin, Germany) using a Plan-Apochromat 40x, 1.2NA water immersion objective. Images of 512x512 pixels per frame were acquired after excitation with a 510 nm pulsed laser diode operating at 20 MHz repetition rate. Fluorescence was split using a 560 nm dichroic mirror and detected by two SPAD detectors, after passing 550/49 nm and 600/50 nm bandpass filters, respectively. The pinhole was set to 1.4 AU. In each measurement, a minimum of 10^5 photons at peak were recorded by accumulation of ca. 30 frames over a time period of 120 s. FLIM data were analysed using SymPhoTime64 software (PicoQuant GmbH, Berlin, Germany). A dual-exponential function was fitted to the decay curves recorded in each pixel, pooled from both detection channels. The short lifetime component was fixed to the average value (ca. 0.9 ns in Xenopus explants, ca. 1.5 ns in gastruloids) obtained by fitting a dual exponential function to the decay curve recorded on the whole image. The second, long-lifetime component was extracted to generate the presented FLIM Flipper tension maps.

Two-photon microscopy

Two-photon imaging of gastruloids was performed on a Zeiss 510 NLO (Inverse - LSM) system (Carl Zeiss, Oberkochen, Germany) using a Plan-Apochromat 40x, 1.2NA water immersion objective. Fluorescence was excited using a femtosecond laser (Laser Mai Tai, DeepSee HP) and detected using two non-descanned GaAsP detectors (channel 1: 500-550 nm, channel 2: 575-640 nm). Per gastruloid, the same 2D plane was imaged at 800 nm to 1040 nm wavelength, in 20 nm intervals. To minimize sample movement, the imaging was performed at room temperature. The detected intensity values were normalized by the effective laser powers recorded using a power meter to correct for wavelength dependent variations of the laser output power.

MDCK monolayers in an alginate tube

Alginate tubes were produced using a microfluidic device[32]. Briefly, 2.5% w/v sodium alginate (Protanal LF200S, FMC corporation, Philadelphia, USA), sorbitol (56755, Merck, Darmstadt, Germany) and a Matrigel (354234, Lot #5173011, Corning)/cell solution were injected in a 3D

657 printed chip with three co-axial channels and the cell solution was incapsulated in the tubes by
658 immersing the tip of the device in a gelation bath with 0.1 M calcium chloride (449709, Sigma-
659 Aldrich, St Louis, USA), and pre-warmed to 37°C.
660
661 **MDCK monolayers in a PDMS roll**
662 PDMS rolls were produced with a self-rolling thin bilayer[39]. Briefly, a toluene (T/2300/15,
663 Fisher Chemical, New Jersey, USA)/PDMS (10 wt% of curing agent, Sylgard 184, Dow
664 Corning, Michigan, USA) solution and a toluene/silicon oil (47 V 350, VWR, Pennsylvania,
665 USA)/PDMS solution were successively spincoated, after reticulation (110°C, 30 min), on a
666 fish gelatin-coated (G7041, Sigma Aldrich, Missouri, USA) PDMS substrate. After the silicon
667 oil extraction in isopropanol (P/7500/15, Fisher Chemical) overnight, fibronectin (33016015,
668 Gibco, New York, USA) was incubated at the surface to allow a cell adhesive surface. Once
669 the monolayer was formed and the Flipper-TR probe was incubated, the PDMS bilayer was cut
670 with a scalpel in the central region, producing two symmetric tubes and forcing the cell
671 monolayer to roll.
672
673 **Gastruloid preparation**
674 A complete description of the culture conditions and the protocol for making gastruloids is
675 presented in Baillie- Johnson et al., 2015[40]. In the experiments presented here, gastruloids were
676 generated from E14Tg2a.4 mouse embryonic stem cells (mESC) (MMRRC, University of
677 California Davis, US) using an initial cell number of 100, and cultured according to the
678 modified protocol described in Hashmi et al., 2022[41]. After 2 days of culture, gastruloids were
679 incubated for 1h in culture medium supplemented with 1 µM Flipper-TR, and transferred to 35
680 mm culture dishes (MatTek Corp., Ashland, MA) for FLIM performed at 37°C, or two-photon
681 imaging. Successful, homogeneous Flipper-TR staining of gastruloids was achieved at
682 different time points of culture (tested and verified between 24h and 96h).
683
684 **Preparation of *Xenopus laevis* animal pole explants**
685 Ovulation was stimulated in *Xenopus laevis* adult females by injection of Human Chorionic
686 Gonadotropin (ChorulonR, 800 units/animal). On the following day, eggs were recovered by
687 squeezing, fertilized *in vitro* with sperm from Nasco males, de-jellied in 2% cysteine
688 hydrochloride (pH 8.0) and washed, first in water, then in 0.1X MBS (Modified Barth's Saline).
689 Embryos were kept in 0.1X MBS at 13°C or 18°C until they reached the desired stage. Animal
690 cap explants were dissected at stage 8.5-9 as previously described[42] and kept in 0.5X MBS

691 solution supplemented with 10 ng/ml Activin (RnD systems).
692 Explants were transferred to a lipidure coated 35 mm culture dish (MatTek Corp., Ashland,
693 MA), stained for 1h in medium supplemented with 1 µM Flipper-TR and stabilized for imaging
694 using a viscous medium, 0.5X MBS supplemented with 1% methylcellulose. Due to the limited
695 penetration of light into the specimen, FLIM was performed in the first cell layer. The
696 experiments were performed at room temperature.
697
698 **Preparation of mouse embryo**
699 Wildtype BALB/c mouse embryos at E6.5 were stained with 1 µM Flipper-TR (Spirochrome)
700 for 2h as described in detail previously[16]. Imaging was performed at 37°C on a Leica SP8
701 equipped with a FALCON module. Fluorescence was excited using a 20x multi-immersion
702 objective (Leica Microsystems) at 488 nm (white light laser, pulsing at 20 MHz) and recorded
703 on the internal HyD-SMD detector (500-700 nm). Image size was 387.63 x 387.63 µm2.
704 Images were processed in LAS-X (Leica Microsystems), thresholded to reject background
705 photons, and binned by a factor of 6 to increase signal-to-noise ratio. The FLIM images were
706 generated using the Phasor-FLIM analysis workflow. The Phasor data were median filtered
707 (window of 5) and a rainbow look up table applied between 3.75 ns and 4.75 ns lifetime (phasor
708 space). The image was exported as RGB for visualization purposes. Quantitative analysis
709 should be performed on exported lifetime images.

Bibliography

(1) Roca-Cusachs, P.; Conte, V.; Trepat, X. Quantifying Forces in Cell Biology. *Nat. Cell Biol.* **2017**, *19* (7), 742–751. https://doi.org/10.1038/ncb3564.

(2) Abella, M.; Andruck, L.; Malengo, G.; Skruzny, M. Actin-Generated Force Applied during Endocytosis Measured by Sla2-Based FRET Tension Sensors. *Dev. Cell* **2021**, *56* (17), 2419-2426.e4. https://doi.org/10.1016/j.devcel.2021.08.007.

(3) Déjardin, T.; Carollo, P. S.; Sipieter, F.; Davidson, P. M.; Seiler, C.; Cuvelier, D.; Cadot, B.; Sykes, C.; Gomes, E. R.; Borghi, N. Nesprins Are Mechanotransducers That Discriminate Epithelial-Mesenchymal Transition Programs. *J. Cell Biol.* **2020**, *219* (10), e201908036. https://doi.org/10.1083/jcb.201908036.

(4) Li, W.; Yu, X.; Xie, F.; Zhang, B.; Shao, S.; Geng, C.; Aziz, A. ur R.; Liao, X.; Liu, B. A Membrane-Bound Biosensor Visualizes Shear Stress-Induced Inhomogeneous Alteration of Cell Membrane Tension. *iScience* **2018**, *7*, 180–190. https://doi.org/10.1016/j.isci.2018.09.002.

(5) Páez-Pérez, M.; López-Duarte, I.; Vyšniauskas, A.; Brooks, N. J.; Kuimova, M. K. Imaging Non-Classical Mechanical Responses of Lipid Membranes Using Molecular Rotors. *Chem Sci* **2021**, *12* (7), 2604–2613. https://doi.org/10.1039/D0SC05874B.

(6) Assies, L.; García-Calvo, J.; Piazzolla, F.; Sanchez, S.; Kato, T.; Reymond, L.; Goujon, A.; Colom, A.; López-Andarias, J.; Straková, K.; Mahecic, D.; Mercier, V.; Riggi, M.; Jiménez-Rojo, N.; Roffay, C.; Licari, G.; Tsemperouli, M.; Neuhaus, F.; Fürstenberg, A.; Vauthey, E.; Hoogendoorn, S.; Gonzalez-Gaitan, M.; Zumbuehl, A.; Sugihara, K.; Gruenberg, J.; Riezman, H.; Loewith, R.; Manley, S.; Roux, A.; Winssinger, N.; Sakai, N.; Pitsch, S.; Matile, S. Flipper Probes for the Community. *Chim. Int. J. Chem.* **2021**, *75* (12), 1004–1011. https://doi.org/10.2533/chimia.2021.1004.

(7) Soleimanpour, S.; Colom, A.; Derivery, E.; Gonzalez-Gaitan, M.; Roux, A.; Sakai, N.; Matile, S. Headgroup Engineering in Mechanosensitive Membrane Probes. *Chem. Commun.* **2016**, *52* (100), 14450–14453. https://doi.org/10.1039/C6CC08771J.

(8) Colom, A.; Derivery, E.; Soleimanpour, S.; Tomba, C.; Molin, M. D.; Sakai, N.; González-Gaitán, M.; Matile, S.; Roux, A. A Fluorescent Membrane Tension Probe. *Nat. Chem.* **2018**, *10* (11), 1118–1125. https://doi.org/10.1038/s41557-018-0127-3.

(9) Mercier, V.; Larios, J.; Molinard, G.; Goujon, A.; Matile, S.; Gruenberg, J.; Roux, A. Endosomal Membrane Tension Regulates ESCRT-III-Dependent Intra-Lumenal Vesicle Formation. *Nat. Cell Biol.* **2020**, *22* (8), 947–959. https://doi.org/10.1038/s41556-020-0546-4.

(10) Roffay, C.; Molinard, G.; Kim, K.; Urbanska, M.; Andrade, V.; Barbarasa, V.; Nowak, P.; Mercier, V.; García-Calvo, J.; Matile, S.; Loewith, R.; Echard, A.; Guck, J.; Lenz, M.; Roux, A. Passive Coupling of Membrane Tension and Cell Volume during Active Response of Cells to Osmosis. *Proc. Natl. Acad. Sci.* **2021**, *118* (47). https://doi.org/10.1073/pnas.2103228118.

(11) Lachuer, H.; Le, L.; Lévêque-Fort, S.; Goud, B.; Schauer, K. Membrane Tension Spatially Organizes Lysosomal Exocytosis. bioRxiv April 22, 2022, p 2022.04.22.489160. https://doi.org/10.1101/2022.04.22.489160.

(12) Goujon, A.; Colom, A.; Straková, K.; Mercier, V.; Mahecic, D.; Manley, S.; Sakai, N.; Roux, A.; Matile, S. Mechanosensitive Fluorescent Probes to Image Membrane Tension in Mitochondria, Endoplasmic Reticulum, and Lysosomes. *J. Am. Chem. Soc.* **2019**, *141* (8), 3380–3384. https://doi.org/10.1021/jacs.8b13189.

(13) Dal Molin, M.; Verolet, Q.; Colom, A.; Letrun, R.; Derivery, E.; Gonzalez-Gaitan, M.; Vauthey, E.; Roux, A.; Sakai, N.; Matile, S. Fluorescent Flippers for Mechanosensitive Membrane Probes. *J. Am. Chem. Soc.* **2015**, *137* (2), 568–571. https://doi.org/10.1021/ja5107018.

(14) Davidson, N. M.; Gallimore, P. J.; Bateman, B.; Ward, A. D.; Botchway, S. W.; Kalberer, M.; Kuimova, M. K.; Pope, F. D. Measurement of the Fluorescence Lifetime of GFP in High Refractive Index Levitated Droplets Using FLIM. *Phys. Chem. Chem. Phys.* **2020**, *22* (26), 14704–14711. https://doi.org/10.1039/C9CP06395A.

(15) Licari, G.; Strakova, K.; Matile, S.; Tajkhorshid, E. Twisting and Tilting of a Mechanosensitive Molecular Probe Detects Order in Membranes. *Chem. Sci.* **2020**, *11* (22), 5637–5649. https://doi.org/10.1039/D0SC02175J.

(16) Royer, C.; Sandham, E.; Slee, E.; Schneider, F.; Lagerholm, C. B.; Godwin, J.; Veits, N.; Hathrell, H.; Zhou, F.; Leonavicius, K.; Garratt, J.; Narendra, T.; Vincent, A.; Jones, C.; Child, T.; Coward, K.; Graham, C.; Fritzsche, M.; Lu, X.; Srinivas, S. ASPP2 Maintains the Integrity of Mechanically Stressed Pseudostratified Epithelia during Morphogenesis. *Nat. Commun.* **2022**, *13* (1), 941. https://doi.org/10.1038/s41467-022-28590-4.

(17) Piazzolla, F.; Mercier, V.; Assies, L.; Sakai, N.; Roux, A.; Matile, S. Fluorescent Membrane Tension Probes for Early Endosomes. *Angew. Chem.* **2021**, *133* (22), 12366–12371. https://doi.org/10.1002/ange.202016105.

(18) García-Calvo, J.; López-Andarias, J.; Maillard, J.; Mercier, V.; Roffay, C.; Roux, A.; Fürstenberg, A.; Sakai, N.; Matile, S. HydroFlipper Membrane Tension Probes: Imaging Membrane Hydration and Mechanical Compression Simultaneously in Living Cells. *Chem. Sci.* **2022**, *13* (7), 2086–2093.

https://doi.org/10.1039/d1sc05208j.
(19) García-Calvo, J.; Maillard, J.; Fureraj, I.; Strakova, K.; Colom, A.; Mercier, V.; Roux, A.; Vauthey, E.; Sakai, N.; Fürstenberg, A.; Matile, S. Fluorescent Membrane Tension Probes for Super-Resolution Microscopy: Combining Mechanosensitive Cascade Switching with Dynamic-Covalent Ketone Chemistry. *J. Am. Chem. Soc.* **2020**, *142* (28), 12034–12038. https://doi.org/10.1021/jacs.0c04942.
(20) López-Andarias, J.; Eblighatian, K.; Pasquer, Q. T. L.; Assies, L.; Sakai, N.; Hoogendoorn, S.; Matile, S. Photocleavable Fluorescent Membrane Tension Probes: Fast Release with Spatiotemporal Control in Inner Leaflets of Plasma Membrane, Nuclear Envelope, and Secretory Pathway. *Angew. Chem. Int. Ed.* **2022**, *61* (1), e202113163. https://doi.org/10.1002/anie.202113163.
(21) Gao, D.; Barber, P. R.; Chacko, J. V.; Sagar, M. A. K.; Rueden, C. T.; Grislis, A. R.; Hiner, M. C.; Eliceiri, K. W. FLIMJ: An Open-Source ImageJ Toolkit for Fluorescence Lifetime Image Data Analysis. *PLOS ONE* **2020**, *15* (12), e0238327. https://doi.org/10.1371/journal.pone.0238327.
(22) Warren, S. C.; Margineanu, A.; Alibhai, D.; Kelly, D. J.; Talbot, C.; Alexandrov, Y.; Munro, I.; Katan, M.; Dunsby, C.; French, P. M. W. Rapid Global Fitting of Large Fluorescence Lifetime Imaging Microscopy Datasets. *PLOS ONE* **2013**, *8* (8), e70687. https://doi.org/10.1371/journal.pone.0070687.
(23) Köllner, M.; Wolfrum, J. How Many Photons Are Necessary for Fluorescence-Lifetime Measurements? *Chem. Phys. Lett.* **1992**, *200* (1), 199–204. https://doi.org/10.1016/0009-2614(92)87068-Z.
(24) Parasassi, T.; Gratton, E.; Yu, W. M.; Wilson, P.; Levi, M. Two-Photon Fluorescence Microscopy of Laurdan Generalized Polarization Domains in Model and Natural Membranes. *Biophys. J.* **1997**, *72* (6), 2413–2429.
(25) Zlotek-Zlotkiewicz, E.; Monnier, S.; Cappello, G.; Le Berre, M.; Piel, M. Optical Volume and Mass Measurements Show That Mammalian Cells Swell during Mitosis. *J. Cell Biol.* **2015**, *211* (4), 765–774. https://doi.org/10.1083/jcb.201505056.
(26) Fischer-Friedrich, E.; Hyman, A. A.; Jülicher, F.; Müller, D. J.; Helenius, J. Quantification of Surface Tension and Internal Pressure Generated by Single Mitotic Cells. *Sci. Rep.* **2014**, *4* (1), 1–8. https://doi.org/10.1038/srep06213.
(27) Stewart, M. P.; Helenius, J.; Toyoda, Y.; Ramanathan, S. P.; Muller, D. J.; Hyman, A. A. Hydrostatic Pressure and the Actomyosin Cortex Drive Mitotic Cell Rounding. *Nature* **2011**, *469* (7329), 226–230. https://doi.org/10.1038/nature09642.
(28) Storck, E. M.; Özbalci, C.; Eggert, U. S. Lipid Cell Biology: A Focus on Lipids in Cell Division. *Annu. Rev. Biochem.* **2018**, *87*, 839–869. https://doi.org/10.1146/annurev-biochem-062917-012448.
(29) Atilla-Gokcumen, G. E.; Muro, E.; Relat-Goberna, J.; Sasse, S.; Bedigian, A.; Coughlin, M. L.; Garcia-Manyes, S.; Eggert, U. S. Dividing Cells Regulate Their Lipid Composition and Localization. *Cell* **2014**, *156* (3), 428–439. https://doi.org/10.1016/j.cell.2013.12.015.
(30) Andrade, V.; Bai, J.; Gupta-Rossi, N.; Jimenez, A. J.; Delevoye, C.; Lamaze, C.; Echard, A. Caveolae Promote Successful Abscission by Controlling Intercellular Bridge Tension during Cytokinesis. *Sci. Adv.* *8* (15), eabm5095. https://doi.org/10.1126/sciadv.abm5095.
(31) Di Meglio, I.; Trushko, A.; Guillamat, P.; Blanch-Mercader, C.; Abuhattum, S.; Roux, A. Pressure and Curvature Control of the Cell Cycle in Epithelia Growing under Spherical Confinement. *Cell Rep.* **2022**, *40* (8), 111227. https://doi.org/10.1016/j.celrep.2022.111227.
(32) Maechler, F. A.; Allier, C.; Roux, A.; Tomba, C. Curvature-Dependent Constraints Drive Remodeling of Epithelia. *J. Cell Sci.* **2019**, *132* (4), jcs222372. https://doi.org/10.1242/jcs.222372.
(33) Chiaruttini, N.; Redondo-Morata, L.; Colom, A.; Humbert, F.; Lenz, M.; Scheuring, S.; Roux, A. Relaxation of Loaded ESCRT-III Spiral Springs Drives Membrane Deformation. *Cell* **2015**, *163* (4), 866–879. https://doi.org/10.1016/j.cell.2015.10.017.
(34) Kang, M.; Day, C. A.; Kenworthy, A. K.; DiBenedetto, E. Simplified Equation to Extract Diffusion Coefficients from Confocal FRAP Data. *Traffic* **2012**, *13* (12), 1589–1600. https://doi.org/10.1111/tra.12008.
(35) Sezgin, E.; Kaiser, H.-J.; Baumgart, T.; Schwille, P.; Simons, K.; Levental, I. Elucidating Membrane Structure and Protein Behavior Using Giant Plasma Membrane Vesicles. *Nat. Protoc.* **2012**, *7* (6), 1042–1051. https://doi.org/10.1038/nprot.2012.059.
(36) Urbančič, I.; Schiffelers, L.; Jenkins, E.; Gong, W.; Santos, A. M.; Schneider, F.; O'Brien-Ball, C.; Vuong, M. T.; Ashman, N.; Sezgin, E.; Eggeling, C. Aggregation and Mobility of Membrane Proteins Interplay with Local Lipid Order in the Plasma Membrane of T Cells. *FEBS Lett.* **2021**, *595* (16), 2127–2146. https://doi.org/10.1002/1873-3468.14153.
(37) Schneider, F.; Waithe, D.; Lagerholm, B. C.; Shrestha, D.; Sezgin, E.; Eggeling, C.; Fritzsche, M. Statistical Analysis of Scanning Fluorescence Correlation Spectroscopy Data Differentiates Free from Hindered Diffusion. *ACS Nano* **2018**, *12* (8), 8540–8546. https://doi.org/10.1021/acsnano.8b04080.
(38) Schindelin, J.; Arganda-Carreras, I.; Frise, E.; Kaynig, V.; Longair, M.; Pietzsch, T.; Preibisch, S.; Rueden, C.; Saalfeld, S.; Schmid, B.; Tinevez, J.-Y.; White, D. J.; Hartenstein, V.; Eliceiri, K.; Tomancak, P.; Cardona, A. Fiji: An Open-Source Platform for Biological-Image Analysis. *Nat. Methods* **2012**, *9* (7), 676–682.

https://doi.org/10.1038/nmeth.2019.
(39) Tomba, C.; Luchnikov, V.; Barberi, L.; Blanch-Mercader, C.; Roux, A. Epithelial Cells Adapt to Curvature Induction via Transient Active Osmotic Swelling. *Dev. Cell* **2022**, *57* (10), 1257-1270.e5. https://doi.org/10.1016/j.devcel.2022.04.017.
(40) Baillie-Johnson, P.; van den Brink, S. C.; Balayo, T.; Turner, D. A.; Arias, A. M. Generation of Aggregates of Mouse Embryonic Stem Cells That Show Symmetry Breaking, Polarization and Emergent Collective Behaviour In Vitro. *JoVE J. Vis. Exp.* **2015**, *2015* (105), e53252. https://doi.org/10.3791/53252.
(41) Hashmi, A.; Tlili, S.; Perrin, P.; Lowndes, M.; Peradziryi, H.; Brickman, J. M.; Martínez Arias, A.; Lenne, P.-F. Cell-State Transitions and Collective Cell Movement Generate an Endoderm-like Region in Gastruloids. *eLife* **2022**, *11*. https://doi.org/10.7554/ELIFE.59371.
(42) Symes, K.; Smith, J. C. Gastrulation Movements Provide an Early Marker of Mesoderm Induction in Xenopus Laevis. *Development* **1987**, *101* (2), 339–349. https://doi.org/10.1242/DEV.101.2.339.